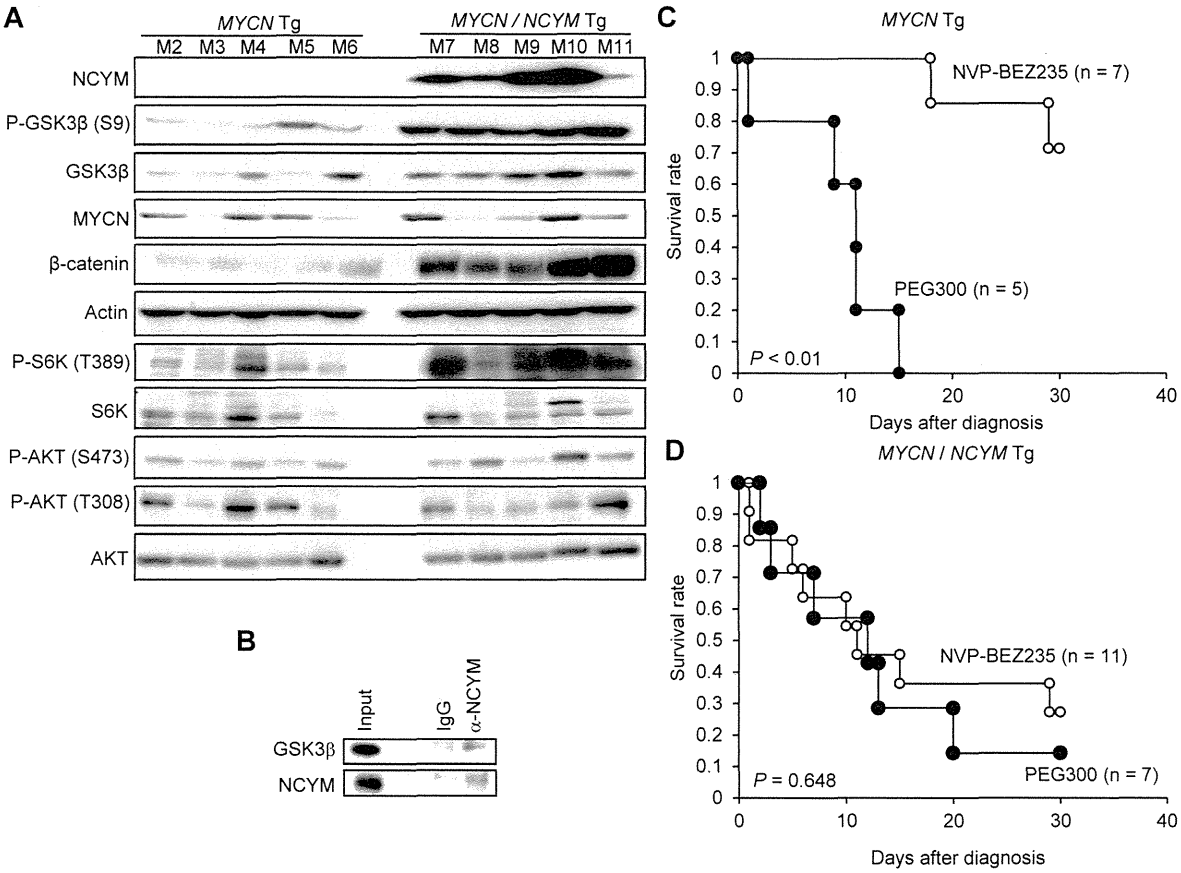

Figure 5. *MYCN/NCYM* tumors show drug resistance to a PI3K/mTOR-dual inhibitor. (A) Western blots of *MYCN* (M2–M6) and *MYCN/NCYM* (M7–M11) mouse tumors for NCYM, phospho-GSK3β (S9), GSK3β, β-catenin, and MYCN, phospho-S6K (T389), S6K, phospho-AKT (S473), phospho-AKT (T308), and AKT. Actin was used as loading control. (B) NCYM binds to GSK3β *in vivo*. Tumors developed in *MYCN/NCYM* transgenic mice (M12) were immunoprecipitated with control IgG or NCYM antibodies. GSK3β was co-immunoprecipitated with a NCYM antibody. (C, D) Kaplan–Meier survival analysis of *MYCN* mice (panel C, $P<0.01$, log-rank test) or *MYCN/NCYM* mice (panel D, $P=0.648$, log-rank test). Treatment with NVP-BEZ235 (35 mg/kg; open circles) or vehicle (PEG300; closed circles). NVP-BEZ235, *MYCN* transgenic mice n = 7, *MYCN/NCYM* transgenic mice n = 11; PEG300, *MYCN* transgenic mice n = 5, *MYCN/NCYM* transgenic mice n = 7.
doi:10.1371/journal.pgen.1003996.g005

Recently, Schramm *et al.* reported that MYCN transcriptionally regulates the mTOR pathway, promoting its activation [33]. Thus, MYCN might have enhanced S6K phosphorylation by activating the mTOR pathway in neuroblastomas caused in the double transgenic mice. Previous reports have suggested that neuroblastoma cell lines expressing high levels of MYCN were significantly more sensitive to mTOR inhibitors compared with cell lines expressing low MYCN levels [34]. Furthermore, our study showed that NCYM knockdown significantly induces apoptosis in *MYCN*-amplified neuroblastoma cells, whereas the effects were marginal in *MYCN*-single neuroblastoma cells. Therefore, the feedback regulation between mTOR-S6K signaling and MYCN/NCYM may contribute to the survival of *MYCN*-amplified neuroblastoma cells (Figure S18).

Although NCYM inhibits GSK3β-mediated MYCN phosphorylation *in vitro*, our data does not rule out the possibility that NCYM may stabilize MYCN in a GSK3β-independent manner. Because NCYM binds directly to MYCN both *in vitro* and in neuroblastoma cells, this may affect the recruitment of the regulators of MYCN stability. Indeed, we have recently found that the tumor suppressor protein Runx3 directly binds to MYCN in neuroblastoma cells and promotes degradation of MYCN in the ubiquitin–proteasome system dependent manner [35]. Therefore, the binding of NCYM to MYCN itself could affect the interaction of Runx3, or other regulators such as Aurora A [36] with MYCN to induce its stability. Further studies are required to evaluate the role of NCYM-mediated inhibition of GSK3β activity on MYCN stability.

Recent reports have suggested that both mutant ALK [37,38] and Lin28B [39] promote the growth of neuroblastomas in transgenic mouse models by targeting MYCN for stabilization [37,38] or overexpression [39]. Among the known regulators of MYCN, *NCYM* is the only gene that shows 100% co-amplification with *MYCN* in human primary neuroblastomas. Overexpressed NCYM stabilizes both MYCN and β-catenin, and enhances the generation of neuroblastomas with increased aggressive behavior such as distant metastasis and/or drug resistance, which are characteristics reminiscent of human neuroblastoma. Recently, Valentijn *et al.* suggested that the activation of the MYCN pathway is a more significant prognostic factor than the expression or amplification of MYCN in primary neuroblastomas [40]. Consistent with this, our results indicate that *NCYM* expression is

associated with poor outcomes in human neuroblastoma regardless of genomic status of the *MYCN/NCYM* locus. Therefore, we anticipate that the positive auto-regulatory loop formed by MYCN and NCYM may be a promising target for developing novel therapeutic tools against high-risk neuroblastoma.

As suggested in the recent report [37], the concomitant inhibition of apoptosis and/or activation of survival signals may be required for MYCN to induce multiple tumors or metastases *in vivo*. In this study, we found that NCYM maintains the survival of *MYCN*-amplified neuroblastoma cells, and that the apoptotic cell number, indicated by cleaved caspase-3, was downregulated in *MYCN/NCYM* transgenic mice. In addition, GSK3β inhibition contributes to the inhibition of apoptosis in response to treatment with DNA-damaging drugs in neuroblastoma cells [41]. Therefore, the concomitant activation of other GSK3β substrates, such as β-catenin, and mTOR-S6K signaling by NCYM may be involved in the inhibition of apoptosis (Figure S18).

Since the proposals of Ohno and Jacob, the birth of a new gene has been believed to be caused by the duplication or rearrangement of pre-existing genes [1,2]. The recent advances in whole genome sequencing technology and bioinformatics have identified the presence of *de novo* proteins; however, their physiological or pathological significance have largely remained unclear [3,15]. In 2010, Li *et al.* reported that MDF1 originated *de novo* from a DNA sequence previously thought to be non-coding in *Saccharomyces cerevisiae* [7]. MDF1 inhibits mating efficiency by binding MATα2 and promoting vegetative growth. Therefore, while MDF1 was the first reported *de novo* gene whose protein product function was unveiled in a monad, NCYM may be the first *de novo* protein whose precise function has been clarified in multicellular organisms, specifically in humans.

In conclusion, NCYM is a *de novo* evolved protein which acts as an oncopromoting factor in human neuroblastoma. Our results suggest that *de novo* evolved new gene products may be involved in the functional regulation of human cancers and even other diseases.

Materials and Methods

Evolutionary analyses

DNA sequences of all species were extracted from the UCSC genome browser on the basis of conservation. From the protein-coding regions, we took the conserved block that was annotated as the region corresponding to the *NCYM* coding sequence, located in exon 3. For intron sequences, we used BLAT [42] to align the *NCYM* mRNA sequence (NR_026766) to the genome of each species and extracted the unmapped regions in the alignment. We found exactly two unmapped regions for each species except for mouse (and thus did not use the mouse sequence). For intergenic regions, we used multiz [43] alignment across 48 species in the browser and cut out 1000-bp sequences that corresponded to human intergenic regions. The sequences of common ancestors were estimated based on the maximum parsimony principle that led to the minimum number of nucleotide-base changes along the already-known phylogenetic tree of the five primates and mice [16]. For multiple possibilities with the same minimum number, we broke the tie by selecting the nucleotide base of the closest outgroup (*e.g.*, when we had A for human, T for chimpanzee, and T for orangutan, we chose T for the common ancestor of human and chimpanzee). When multiple possibilities still remained (as in common ancestor 1), we considered all the possibilities to be equally probable. We estimated common ancestor sequences only within close species (human, chimpanzee, orangutan, and rhesus macaque). We used BLAST [44] to make an alignment between two translated amino-acid sequences ending at the first terminal codon, and calculated K_a and K_s using the KaKs_Calculator [45] with the 'gMYN' method, where K_a and K_s are the rates of non-synonymous and synonymous amino-acid changes, respectively. All pairs of sequences were aligned entirely from the start codon to the terminal codon and did not include any indels, except for the alignment between common ancestor 2 and common ancestor 3, for which we noted 'frameshift' instead of the K_a and K_s values.

We measured a bias in the codon frequencies (or amino acid frequencies) through the deviation from the uniform usage of each codon, using the Chi-squared statistic normalized to the number of codons:

$$\text{Bias} = \left(\sum_{i=1}^{k} \frac{\left(n_i - \frac{N}{k}\right)^2}{\frac{N}{k}} \right) / k,$$

where n_1, …, n_k ($n_i \neq 0$) are the observed number of codon 1, …, and that of codon k, respectively. N is $n_1 + \ldots + n_k$. We used R for the calculations and computed the P-values using a Monte-Carlo simulation with 10,000 replicates.

Generation of a human NCYM antibody

A polyclonal anti-NCYM antibody was raised in rabbits against a 14-amino acid stretch at the C-terminal region of NCYM (84-LGTRPLDVSSFKLK-97) (Medical and Biological Laboratories, Nagoya, Japan). The specificity of the purified antibody's affinity was assessed by immunoblotting.

Immunohistochemistry

Neuroblastoma tissues obtained from mice were fixed in 4% paraformaldehyde and paraffin-embedded for histological studies. Tissue sections were stained with hematoxylin and eosin (H&E) and examined histologically by pathologists for confirmation of the tumor type. Tissue arrays (FDA808a-1 and FDA808a-2, US Biomax, Rockville, MD, USA) were used for the analyses of NCYM or MYCN expression in normal and tumorous human tissues. For immunohistochemistry, tissue sections were stained with the polyclonal anti-NCYM antibody we generated, an anti-MYCN antibody (Calbiochem, San Diego, CA, USA), and cleaved Caspase-3 (Cell Signaling Technology).

Immunofluorescence

MYCN-amplified human neuroblastoma TGW cells grown on coverslips were fixed with 4% paraformaldehyde in 1× PBS for 20 min at 4°C, permeabilized with 0.1% Triton-X for 20 min at room temperature, and then incubated with 2% BSA and 3% goat serum in PBS for 1 h to reduce nonspecific binding. Immunostaining was performed by incubating cells with the polyclonal anti-NCYM antibody and a monoclonal anti-MYCN antibody (Calbiochem) for 2 h at room temperature in a humidified chamber, followed by incubation with fluorescent-conjugated goat anti-rabbit IgG (diluted 1:400) or fluorescent-conjugated goat anti-mouse IgG (diluted 1:400), respectively. The coverslips were washed extensively with PBS, mounted in VECTASHIELD mounting medium with DAPI (Vector Laboratories, Burlingame, CA, USA) and images were captured using a confocal microscope (DMI 4000B, Leica).

Plasmids

We previously made a MYCN-luc (+1312) plasmid that contains the region of MYCN promoter region spanning from −221 to +1312 (where +1 represents the transcription start site) [27]. Luciferase reporter plasmids containing different lengths of

the MYCN promoter were generated from MYCN-Luc (+1312) by partial removals of the *MYCN* promoter region with appropriate restriction enzymes. The MYCN promoter region in MYCN-luc (+1312) was subcloned into the pGL3basic vector or pGL4.17Δ*Eco*RV *Eco*RI vector in the opposite direction for generation of NCYM-luc vectors. pGL4.17 Δ*Eco*RV *Eco*RI was the luciferase reporter plasmid, where an *Eco*RV site in pGL4.17 (Promega, Southampton, UK) is replaced with an *Eco*RI site. NCYM-luc E-box WT and NCYM-luc E-box MT were generated by PCR-based amplification using MYCN-luc (+1312) as a template. Oligonucleotide primers used were as follows: 5′-AACCAGGTTCCCCAATCTTC-3′ (forward) and 5′-ACCACCCCCTGCATCTGCAT-3′ (reverse, NCYM-luc E-box WT) or 5′-ACCACCCCCTGCATCCGCAT-3′ (reverse, NCYM-luc E-box MT). Underlined sequences in the reverse primers indicate the wild-type or mutant E-boxes. The NCYM complementary DNA was introduced into a pcDNA3 expression vector, comprising a FLAG-tag at the 5′ locus of NCYM to generate pcDNA3-FLAG-*NCYM*. The sequence of the entire *NCYM* open reading frame was confirmed by sequencing. The FLAG-*NCYM* cDNA was ligated downstream of the rat *TH* promoter in the pGEM7z(f+) expression plasmid, which was originally made from a *MYCN* transgenic construct [21] by excision of the *MYCN* gene, to generate pGEM7z(f+)-FLAG-*NCYM*.

Cell culture, infection, transfection, and RNA interference

Human neuroblastoma cell lines SH-SY5Y, SK-N-AS, NLF, IMR32, CHP134, and SK-N-BE were maintained in RPMI-1640 medium supplemented with 10% fetal bovine serum (FBS) and antibiotics. Human neuroblastoma cell line BE (2)-C was maintained in a 1:1 mixture of minimal essential medium (MEM, Gibco by Life technologies, Carlsbad, CA, USA) and Ham's Nutrient Mixture F12 (Gibco) supplemented with 15% heat inactivated fetal bovine serum (FBS) (Gibco) with MEM non-essential amino acids (Gibco) and antibiotics. Mouse neuroblastoma cell line Neuro 2a was maintained in DMEM supplemented with 10% FBS and antibiotics. NLF, IMR32, CHP134, SK-N-BE, and BE (2)-C have amplified *MYCN*, whereas SH-SY5Y, SK-N-AS, and Neuro 2a are cell lines with a single copy of *MYCN*. The cells or tissues with a single copy of *MYCN* have one copy of *MYCN* gene in a haploid genome. Lentivirus was produced by co-transfecting cDNA or shRNA expression plasmids with pCMVR and pMDG plasmids into HEK293T cells using FuGENE HD reagent (Roche, Mannheim, Germany). The MYCN and NCYM shRNA expression plasmids contained pLKO.1-puro as the backbone (Sigma, St Louis, MO, USA). At 24 and 48 h after transfection, the viral supernatants were collected and mixed with neuroblastoma cells. Other plasmid transfections were done using Lipofectamine 2000 transfection reagent (Invitrogen, Karlsruhe, Germany) according to the manufacturer's instructions. The target sequences of the shRNAs used were as follows: NCYM sh-1 (N-cym1 custom shRNA, Sigma) 5′-tggcaattgcttgtcattaaa-3′, NCYM sh-2 (N-cym 2 custom shRNA, Sigma) 5′-gaggttgctcctgtgtaatta-3′, NCYM sh-3 (N-cym 3 custom shRNA, Sigma) 5′-tcctgtgtaattacgaaagaa-3′, MYCN sh-1 (TRCN0000020694, Sigma) 5′-gccagtattagactggaagtt-3′, MYCN sh-2 (TRCN0000020695, Sigma) 5′-cagcagcagttgctaaagaaa-3′. The control shRNA (SHC002) was purchased from Sigma.

RNA isolation, RT-PCR and quantitative real-time RT-PCR

Total RNA was isolated from the frozen tumor samples and adrenal tissues of transgenic mice with ISOGEN (NIPPON GENE, Tokyo, Japan), and treated with RNase-free DNase I. Total RNA from neuroblastoma cells (CHP134 and SK-N-AS) was prepared using an RNeasy Mini kit (Qiagen, Valencia, CA) following the manufacturer's instruction. cDNA was synthesized using SuperScript II with random primers (Invitrogen). Quantitative real-time RT-PCR (qRT-PCR) using an ABI PRISM 7500 System (Applied Biosystems, Foster City, CA) was carried out using a SYBR green PCR reaction. The primer sets used were as follows: (for clinical experiments using primary neuroblastomas) human *MYCN*, 5′-ggacaccctgagcgattcag-3′, and 5′-aggaggaacgccgcttct-3′, human *NCYM* 5′-ccgacagctcaaacacagaca-3′ and 5′- gtaatggcttctgcgaaaagaaa-3′; (for cellular experiments) human *MYCN*, 5′-tccatgacagcgctaaacgtt-3′ and 5′- ggaacacacaaggtgacttcaaca-3′, human *NCYM*, 5′-cgcccccttaggaacaagac-3′ and 5′- gcgcccctcttctttcaatt-3′, mouse *MYCN*, 5′-tcgggacactaaggagcttca-3′ and 5′-ggaatcttggaccggaacaa-3′, mouse *GAPDH*, 5′-gggaagcccatcaccatct-3′ and 5′-cggcctcaccccatttg-3′. The mRNA levels of each of the genes were standardized by *β-actin* or *GAPDH*.

Luciferase assay

SK-N-AS cells were co-transfected with the indicated reporter constructs and the pRL-TK *Renilla* luciferase cDNA together with increasing amounts of the expression plasmid for MYCN or MYC. Total DNA per transfection was kept constant (510 ng) by adding pcDNA3 (Invitrogen). Forty-eight hours after transfection, firefly and *Renilla* luciferase activities were measured with a dual-luciferase reporter assay system according to the manufacturer's instructions (Promega).

Immunoblotting

We resolved cell proteins by SDS-PAGE before electro-blotting onto PVDF membranes. We incubated the membranes with the following primary antibodies overnight: anti-NCYM (1:1000 dilution), anti-MYCN antibody (1:1000 dilution; Calbiochem and Cell Signaling), anti-Lamin B (1:1000 dilution; Calbiochem), anti-α-tubulin (1:1000 dilution; Santa Cruz, CA, USA), anti-GST (1:1000; Santa Cruz), anti-GSK3β (1:1000 dilution; Cell Signaling), anti-phospho-GSK3β (S9) (1:1000 dilution; Cell Signaling), anti-β-catenin (1:1000 dilution; Cell Signaling), anti-phospho-AKT (S473) (1:1000 dilution; Cell Signaling), anti-phospho-AKT (S308) (1:1000 dilution; Cell Signaling), anti-AKT (1:1000 dilution; Cell Signaling), anti-S6K (1:1000 dilution; Cell Signaling), anti-phospho-S6K (T389) (1:1000 dilution; Cell Signaling), and anti-actin (1:4000 dilution; Sigma). The membranes were then incubated with a horseradish peroxidase-conjugated secondary antibody (anti-rabbit IgG at 1:2000–1:4000 dilution or anti-mouse IgG at 1:2000 dilution; both from Cell Signaling Technology) and the bound proteins were visualized using a chemiluminescence-based detection kit (ECL and ECL pro kit, Amersham, Piscataway, NJ, USA; ImmunoStar LD, Wako).

Immunoprecipitation

Whole lysates prepared from CHP134 cells or tumor tissues were pre-cleared by incubation with protein G-Sepharose beads (Amersham Pharmacia Biotech) for 1 h at 4°C. The supernatant was collected after a brief centrifugation, and incubated with the indicated primary antibodies at 4°C overnight. The immune complexes were precipitated with protein G-Sepharose beads for 1 h at 4°C, and the non-specific bound proteins were removed by washing the beads with lysis buffer five times at 4°C. Different lysis buffers were used for the cell-based experiments (50 mM Tris-HCl pH 8.0, 137 mM NaCl, 2.7 mM KCl, and 1% Triton X) and for the tumor tissues (50 mM Tris-HCl pH 8.0, 1 mM EDTA, 0.2% DOC and 0.2% SDS). The immunoprecipitated proteins were eluted by boiling in Laemmli sample buffer and analyzed by immunoblotting.

Analysis of MYCN stability

CHP134 cells were cultured with 50% lentiviral supernatant for transfection of the indicated shRNA. Forty-eight hours after the transfection, cycloheximide (Sigma) was added to the culture medium at a final concentration of 50 μg/ml and cells were harvested at the indicated time points. For MG132 treatment, 44 h after the transfection, cells were treated with DMSO or 10 μM MG132 for 4 h.

Purification of NCYM protein from bacteria

DH5α cells were transformed with pGEX-4T-*NCYM* plasmid and cultured in Luria Broth (LB) at 37°C. The expression of the GST-NCYM fusion protein was induced by culturing the cells with 1 mM IPTG for 10 h at 25°C. Cells were collected by centrifugation, dissolved in cell lysis buffer (PBS, 1% TritonX-100, 5 mM EDTA and protease inhibitors), and stored at −80°C. Cell extracts were obtained by thawing the frozen cells, followed by sonication and ultra-centrifugation. After a pulldown with glutathione sepharose 4B beads, the beads were washed five times in cell lysis buffer and once in thrombin buffer containing 50 mM Tris-HCl pH 8.0, 150 mM NaCl, 2.5 mM $CaCl_2$, 5 mM $MgCl_2$, 1 mM DTT. GST-Tag cleavage mediated by thrombin released the full-length NCYM protein from the beads and the thrombin was removed by adding p-aminobenzamidine agarose beads according to the standard protocol. The full length NCYM protein was further purified by filtration using Amicon Ultra-4 (Millipore, Temecula, CA, USA), and dissolved in stock buffer (50 mM Tris-HCl pH 8.0, 150 mM NaCl, 5 mM EDTA, 0.25 mM DTT, 10% sodium azide, 50% glycerol and protease inhibitors) and stored at −20°C. Complete PIC (Roche) was used for protease inhibition.

GST-pulldown assay

For GST-pulldown assay, 0.5 μg of purified NCYM proteins were incubated with 0.5 μg of GST protein or GST-fused CDK1/Cyclin B1 (Signal Chem, Richmond, Canada), GSK3β (Promega) and MYCN (Abnova, Taipei, Taiwan) for 2 h at 4°C. Bound complexes were recovered on the glutathione-sepharose beads, washed with the binding buffer (50 mM Tris-HCl, pH 8.0, 1 mM EDTA, 150 mM NaCl, 0.1% Nonidet P-40 and Complete PIC), boiled in in Laemmli sample buffer and analyzed by immunoblotting.

In vitro kinase assay

For MYCN phosphorylation, two kinase reactions were performed sequentially. The first kinase reactions were performed for 1 h in kinase buffer (40 mM Tris-HCl pH 7.5, 20 mM $MgCl_2$, 0.1 mg/ml BSA, 50 μM DTT) in the presence of 50 μM Ultrapure ATP (Promega), 50 ng of purified MYCN (Abnova), and 40 ng of purified CDK1/Cyclin B1 (Signal Chem) at room temperature. At 1 h, the first reaction solution was mixed with the same volume of kinase buffer containing 100 nM CDK1 inhibitor (CGP74514A, Calbiochem), 4 μCi of [γ-^{32}P] ATP (PerkinElmer), and 20 ng of purified GSK3β with the indicated amounts of purified NCYM or purified GST. The second reaction was performed for 1 h at room temperature. The amount of phosphorylated MYCN was quantified using standard autoradiography. The total amount of MYCN was quantified by using an Oriole Fluorescent Gel stain (Bio-Rad). We also examined whether purified NCYM could be a substrate of GSK3β using the ADP-Glo system (Promega) according to manufacturer's instructions. Reactions were performed for 1 h in kinase buffer (40 mM Tris-HCl pH 7.5, 20 mM $MgCl_2$, 0.1 mg/ml BSA, 50 μM DDT) in the presence of 25 μM Ultrapure ATP (Promega) and 25 ng of purified GSK3β with increasing amounts of NCYM or GST at room temperature. The peptide of human muscle glycogen synthase-1 (YRRAAVPPSPSLSRHSSPHQ(pS)EDEEE) was used as a positive control for the GSK3β substrate. At 1 h, the reaction solutions were mixed and incubated with ADP-Glo reagent for 40 min at room temperature, and the mixture was combined with a kinase detection reagent and allowed to stand for 30 min. The kinase activities were detected using a luminometer (PerkinElmer ARVOX3).

TUNEL staining

The indicated neuroblastoma cells were transfected with the indicated shRNA with 50% lentiviral supernatant. Seventy-two hours after transfection, all cells were collected by centrifugation, attached onto the coverslips by CYTOSPIN 4 (Thermo Fisher Scientific, Wilmington, DE, USA), and fixed in 4% paraformaldehyde for 1 h. Apoptotic cells were detected by using an *in situ* cell death detection kit (Roche) according to the manufacturer's protocol. The coverslips were mounted with DAPI-containing mounting medium (Vector Laboratories) and observed under a confocal microscope.

Cell viability assay (MTT assay)

Cell viability was quantified by the 3-(4, 5-dimethylthiazol-2-yl)-2, 5-diphenyltetrazolium bromide (MTT) method. Cells were collected and seeded in 96-well plates at 1×10^4 cells/ml. After addition of 10 μl of MTT tetrazolium salt (Sigma) solution to each well, the plates were incubated in a CO_2 incubator for 60 min. The absorbance of each well was measured using a Dynatech MR5000 plate reader with a test wavelength of 450 nm and a reference wavelength of 630 nm.

Migration and invasion assay

The invasive potential of BE (2)-C cells *in vitro* was measured by evaluating the number of invading cells using Matrigel-coated trans-well inserts (BD Biosciences) according to the manufacturer's instructions. BE (2)-C cells transfected with the indicated shRNA were seeded onto an insert containing 8 μm pores (BD Biosciences) in a 24-well plate at 1×10^5 cells/ml. Cells on the lower side of the membrane were fixed with 4% paraformaldehyde and stained using a Diff Quick Staining Kit (Sysmex).

Generation of transgenic mice

All animal experimental procedures used in this study were reviewed and approved by the Committee on the Ethics of Animal Experiments of the Chiba Cancer Center (Permit Number: 12–13). Linearized and purified pGEM7z (f+)-FLAG-*NCYM* was injected into the pronuclei of fertilized eggs derived from 129/SvJ×C57BL/6J mice. We selected four lines of *NCYM* transgenic mice according to the level of *NCYM* expression in adrenal tissues (Figure S15B), and the transgenic mice were backcrossed to 129/SvJ at least 10 times to generate *NCYM* transgenic mice. To generate *MYCN/NCYM* double transgenic mice, the *NCYM* transgenic mice were crossed with *MYCN* transgenic mice of the 129/SvJ strain. On the basis of breeding schemas, all mice carrying the *MYCN* transgene were hemizygous. Tail DNA was analyzed for *MYCN* and *NCYM* transgenes, and the *NCYM* transgene copy number was quantified by quantitative genomic PCR. The primer sets used for genotyping were as follows: *NCYM*, 5′-cgccccttaggaacaagac-3′ and 5′- gcgcccctcttctttcaatt-3′, *MYCN*, 5′-tggaaagcttcttattggtagaaacaa-3′ and 5′-agggatcctttccgccccgttcg-ttttaa-3′.

Detection of metastatic tumors in mice

If more than one tumor over 2 mm in a diameter separately developed in a different organ, we defined this as the mouse having macroscopic metastatic tumors. In Figure 4C, only the number of mice with macroscopic metastatic tumors was counted. As a preliminary experiment, we used microscopy to detect tumors in the brain, pancreas, spleen, heart, lungs, kidneys and liver in nine mice (*MYCN/NCYM* double transgenic mice; n = 6, *MYCN* transgenic mice; n = 3). In addition to macroscopic metastases in the brain, heart, ovary and uterus, we found microscopic metastases in the lungs of *MYCN/NCYM* double transgenic mice, but the mass of these tumor cells was not large enough to be visible by eye. We also microscopically analyzed the HE-stained bone marrow from the hind legs of 19 mice (*MYCN/NCYM* double transgenic mice, n = 10; *MYCN* transgenic mice, n = 9). However, no metastatic tumor cells were found in the bone marrow.

Murine therapy

All mice were genotyped to detect the presence of human *MYCN* or *NCYM* transgenes. After weaning, at about 30 days old, *MYCN* transgenic mice or *MYCN/NCYM* double transgenic mice were palpated for intra-abdominal tumors every day. Mice of either genotype found with palpable tumors were treated with NVP-BEZ235 (Cayman Chemical, Ann Arbor, MI, USA) (35 mg/kg in PEG300) or vehicle (PEG300, Wako) once daily for 30 days by oral gavage. All mice were monitored until euthanasia was required in accordance with the institutional animal committee.

Tumor specimens

The 106 human neuroblastoma specimens used in the present study were kindly provided by various institutions and hospitals in Japan to the Chiba Cancer Center Neuroblastoma Tissue Bank. Written informed consent was obtained at each institution or hospital. This study was approved by the Chiba Cancer Center Institutional Review Board. Tumors were classified according to the International Neuroblastoma Staging System (INSS): 27 Stage 1, 15 Stage 2, 34 Stage 3, 23 Stage 4, and 7 Stage 4 s. Clinical information including age at diagnosis, tumor origin, Shimada's histology, prognosis and survival duration of each patient was obtained. The patients were treated following the protocols proposed by the Japanese Infantile Neuroblastoma Cooperative Study and the Group for the Treatment of Advanced Neuroblastoma and subjected to survival analysis. Cytogenetic and molecular biological analysis of all tumors was also performed by assessing DNA ploidy, *MYCN* amplification and *TrkA* expression, as previously described [46].

Array CGH analysis

Array CGH analysis was conducted using the Human Genome CGH 244K Oligo Microarray Kit (G4411B, Agilent Technologies, Santa Clara, CA, USA). Genomic DNA prepared from primary neuroblastoma tissues or cell lines was labeled with Cy3-dye using a QuickAmp labeling kit. Human placental DNA was labeled with Cy5-dye and used as a reference control. Labeling, hybridization and subsequent data processing by FeatureExtraction and CGH-Analytics software were performed according to the manufacturer's instructions. Relative copy number of the probes surrounding the *MYCN* and *NCYM* genomic locus (from *DDX1* to *FAM49A*) were compared in each primary tumor or cell line.

Statistical analysis

Statistical significance was tested as follows: two-group comparison of survival by log-rank test, correlation of gene expression by Pearson's correlation coefficient test or Student's *t*-test, multivariate analysis for survival by Cox regression model, and the rate of mouse genotype and metastatic tumor occurrence in line 6 was calculated by Chi-square independence test and Mann–Whitney U test, respectively.

Supporting Information

Figure S1 Alignment of NCYM coding sequences. Primate sequences were extracted from the UCSC genome browser on the basis of conservation, and common-ancestor sequences were estimated based on the maximum parsimony principle. Nucleotide changes are colored in orange. Post-terminal sequences are colored in blue. Post-terminal sequence refers to the DNA sequence after the first terminal codon up to the position corresponding to the first terminal codon in the human sequence. CA indicates common ancestor.
(TIF)

Figure S2 Analysis of the bias of codon (and amino acid) usage and evolutionary rates in the *NCYM* gene. (A) Distribution of NCYM protein length, numbers of end codons, and the bias of codon and amino acid usage. Asterisk indicates statistical significance ($P<0.001$, Monte-Carlo Chi-square test). Graph showing the number of codons (B) or amino acids (C) in the NCYM protein of different species.
(TIF)

Figure S3 Exogenous NCYM protein can be expressed in cells. (A) Purification of NCYM protein from bacteria. GST fusion NCYM was overexpressed in bacterial cells and purified by GST-pulldown. The GST-NCYM protein was further cleaved by thrombin, and full-length NCYM was purified. The left panel shows CBB staining and the right panel shows a western blot using anti-NCYM antibody. The arrow indicates the NCYM protein; the asterisk indicates the degraded NCYM protein. (B) Human NCYM protein expression in mouse neuroblastoma Neuro 2a cells. Neuro 2a cells were transfected with increasing amounts of NCYM expression plasmid (1, 1.5, 2 μg) for 48 h. The cell lysates were subjected to western blotting to verify the expression of human NCYM using an anti-NCYM antibody. The arrow indicates the NCYM protein; the asterisk indicates a non-specific band.
(TIF)

Figure S4 Subcellular localization of NCYM protein in neuroblastoma cells. (A) Localization of NCYM protein in neuroblastoma cells. The indicated neuroblastoma cells were biochemically fractionated into nuclear and cytoplasmic fractions followed by immunoblotting with anti-NCYM antibody. Lamin B and α-tubulin were used as nuclear and cytoplasmic markers, respectively. SK-N-AS and SH-SY5Y are human neuroblastoma cells with a single copy of *MYCN*, and NLF, IMR32, CHP134, and SK-N-BE are human neuroblastoma cells with amplified *MYCN*. (B) Nuclear staining of NCYM and MYCN protein in *MYCN*-amplified human neuroblastoma TGW cells analyzed by confocal fluorescence microscopy. Scale bar, 50 μm.
(TIF)

Figure S5 NCYM protein expression in human normal and neuroblastoma tissues analyzed by immunohistochemistry. The indicated human normal tissues (tissue array, FDA808a-1) were stained with anti-NCYM antibody. (A) Cerebellum; scale bar, 100 μm. (B) Testis; scale bar, 50 μm. (C) Pancreas; scale bar, 100 μm. (D) Heart; scale bar, 100 μm. (E) Human metastatic neuroblastoma in the liver (Stage 4S); scale bar, 50 μm. (F) Human

metastatic neuroblastoma in the lymph node (Stage 4); scale bar, 50 μm.
(TIF)

Figure S6 Expression of NCYM and MYCN protein in human thyroid tumors analyzed by immunohistochemistry. Normal and cancerous human tissues (tissue array, FDA808a-2) were stained with anti-NCYM (A and B) or anti-MYCN antibody (C and D). (A), (C), Normal thyroid. (B), (D), Thyroid tumors. Scale bars, 100 μm.
(TIF)

Figure S7 Co-amplification of *MYCN* and *NCYM* genes in human neuroblastoma cell lines and primary neuroblastomas. Average gene copy number was calculated based on the signals of multiple probes targeted to the indicated gene in array CGH. Twenty-three *MYCN*-amplified human neuroblastoma cell lines (A) or 23 human primary neuroblastomas (B) were analyzed by array CGH.
(TIF)

Figure S8 High *NCYM* mRNA expression is associated with poor prognosis in neuroblastomas without *MYCN* amplification. *MYCN* non-amplified neuroblastomas diagnosed at over one year of age were analyzed using Kaplan–Meier survival curves based on the expression levels of *NCYM* mRNA (A) or *MYCN* mRNA (B). The expression levels of *NCYM* or *MYCN* mRNA were examined by qRT-PCR and normalized by *GAPDH*. The average of the expression levels was used as a threshold to divide the tumors with low expression (open circle; A, n = 36, B, n = 34) from those with high expression (closed circle; A, n = 9, B, n = 11). *P* values of (A) and (B) were 0.0375 and 0.144, respectively (Log-rank test).
(TIF)

Figure S9 MYCN, but not MYC, activates *MYCN* transcription in human neuroblastoma cells. (A) Schematic drawing of the *MYCN/NCYM* promoter region. (B) Relative mRNA levels of *MYC*, *MYCN* and *NCYM* in SK-N-AS *MYCN* single copy human neuroblastoma cells transfected with 2 μg of a MYC expression vector. mRNA levels were measured by qRT-PCR with *β-actin* as an internal control. (C) Luciferase reporter assays. SK-N-AS cells were transiently co-transfected with a constant amount of the indicated luciferase reporter constructs bearing various lengths of the human *MYCN* promoter region (100 ng), a *Renilla* luciferase reporter plasmid (pRL-TK) (10 ng), and either an empty plasmid (pcDNA3) or with an increasing amount (200, 300, 400 ng) of the expression plasmid for MYCN. Forty-eight hours after transfection, cells were lysed and their luciferase activities were measured.
(TIF)

Figure S10 An intact upstream E-box is required for the activation of the NCYM promoter by MYCN. (A) The NCYM promoter sequence. The sequences of primer sets used in our previous report [27] are shown as MYCN ChIP Forward (Reverse) Primer. The recruitment of the MYCN protein to its own intron 1 was detected using those primers. The putative E-box sequence is indicated in red characters. (B) MYCN, but not MYC, enhances NCYM promoter activity. Human neuroblastoma SK-N-AS cells were transfected with 400 ng of the MYCN expression plasmid for 48 hours and then their luciferase activity was measured. (C) The effect of an E-box mutation on MYCN-induced NCYM promoter activity. The WT and mutant NCYM promoters were evaluated for transcriptional activity 24 hours after the transfection of the expression plasmids for MYCN or MYC. The asterisks indicate statistical significance ($P<0.01$, Student's *t*-test).
(TIF)

Figure S11 NCYM stabilizes the MYCN protein in the ubiquitin–proteasome system dependent manner. (A) Western blot analysis and RT-PCR. Both NCYM and its SNP type (NCYML70V) induce MYCN expression levels in CHP134 cells. (B) Western blot analysis of MYCN expression in CHP134 cells transfected with NCYM or control shRNA, followed by treatment with 50 μM cycloheximide (CHX), and harvested at the indicated time points. (C) Proteasome inhibitor MG132 treatment of NCYM knockdown CHP134 cells. Western blot analysis showed that NCYM-mediated downregulation of MYCN is inhibited by MG132 treatment. Actin was used as a loading control.
(TIF)

Figure S12 GSK3β does not phosphorylate NCYM protein. (A) *In vitro* kinase assay. The phosphorylation of the control substrate human glucose synthase 1 by GSK3β was measured to test the assay system. (B) The correlation between the percentage of ADP and the relative kinase activity measured by luciferase activity ($R^2 = 0.9994$). (C) The relative kinase activity of GSK3β was not increased when GST or NCYM were used as a substrate.
(TIF)

Figure S13 NCYM knockdown promotes apoptosis in *MYCN*-amplified neuroblastoma cells. (A) The relative mRNA levels of *MYCN*, *NCYM* and *MYC* in human neuroblastoma cells. Levels of mRNA were measured by qRT-PCR with *β-actin* as an internal control. (B and C) TUNEL staining. The indicated human neuroblastoma cells were lentivirally transfected with the indicated shRNA. Sevently-two hours after the transfection, cells were fixed in 4% paraformaldehyde and subjected to TUNEL staining. Cell nuclei were stained with DAPI (upper panels). Scale bars, 50 μm. The percentage of TUNEL-positive cells was calculated as the average of three different microscopic fields. SH-SY5Y and SK-N-AS are *MYCN* single copy cells (B), and BE (2)-C and CHP134 are *MYCN*-amplified cells (C).
(TIF)

Figure S14 NCYM knockdown inhibits the proliferation and invasion in BE (2)-C cells. (A) Western blot analysis showed that NCYM knockdown decreased MYCN protein in BE (2)-C cells. (B) Cell proliferation assay. After transfection with NCYM shRNA (closed circle) or control shRNA (open circle), cell proliferation was examined in an MTT assay, at the indicated time points. (C, D) the effect of NCYM knockdown on cellular migration (C) and invasion (D). Three days after the introduction of NCYM shRNA, the cells were adjusted to 1×10^5 cells/ml and subjected to a Boyden chamber invasion assay.
(TIF)

Figure S15 Generation of *MYCN/NCYM* transgenic mice. (A) A *NCYM* cDNA was ligated 3′ to the rat *TH* promoter to generate the pGEM7z(f+)-FLAG-*NCYM* transgenic constructs. (B) *NCYM* mRNA expression in the adrenal tissues of *NCYM* transgenic mice was measured by qRT-PCR. The expression levels were normalized to mouse *GAPDH*. Red arrows indicate the mouse lines used for further experiments. (C) Table showing the distribution of actual numbers of transgenic mice (line 6) resulting from intercrossing of *MYCN* Tg/+ *NCYM* Tg/+ and *NCYM* Tg/+ and the corresponding theoretical numbers ($P>0.05$, Chi-square independence test). This result indicates that the *NCYM* and *MYCN* transgenes have a marginal effect on the embryonic lethality of mice. (D) Kaplan–Meier survival curves of 83 mice resulting from intercrosses of *MYCN* Tg/+ *NCYM* Tg/+ and *NCYM* Tg/+ (mouse line 6). (E) Kaplan–Meier analysis for tumor incidences in *MYCN* Tg/+ and *MYCN/NCYM* Tg mice (mouse line 6).
(TIF)

Figure S16 Neuroblastoma histology of *MYCN* transgenic mice and *MYCN/NCYM* double transgenic mice. (A) Neuroblastomas arise as primary lesions in a *MYCN/NCYM* double transgenic mouse (i) and *MYCN* transgenic mice (ii). Thoracic paraspinal (T1) and abdominal (T2, T3) tumors. K, kidney. (B) H&E staining of T1 (i), T2 (ii), and T3 (iii).
(TIF)

Figure S17 NCYM inhibits apoptosis in the neuroblastomas of *MYCN/NCYM* double transgenic mice. The number of apoptotic cells in neuroblastomas from *MYCN* transgenic mice (A) and *MYCN/NCYM* double transgenic mice (B) were measured using cleaved capase-3 staining. Scale bar, 50 μm. (C) Quantification of cleaved caspase-3–positive areas in the tumors. The apoptotic cells were calculated by averaging the number of cleaved caspase-3–positive areas counted in 5 randomly selected fields (100 μm^2) per slide using WinROOF software (version 7.0, Mitani Corp.). *P* value was 0.012 (Student's *t*-test).
(TIF)

Figure S18 Schematic model of NCYM function in aggressive human neuroblastomas.
(TIF)

Table S1 Correlation between the expression of *NCYM* or *MYCN* and other prognostic factors.
(DOC)

Table S2 Multiple Cox regression analyses of *NCYM* expression, *MYCN* expression, age, *MYCN* amplification, stage, DNA index, Shimada pathology, *TrkA* expression, and origin.
(DOC)

Table S3 Summary of mice bearing neuroblastomas.
(DOC)

Acknowledgments

We thank I. Kuroita, H. Nakamura, and Y. Nakamura for their technical support in the computational data analyses, A. Sada and N. Kitabayashi for DNA and RNA extractions, R. Murasugi for FISH analyses support, T. Ozaki, T. Kamijo, Y. Yamaguchi, Y. Tatsumi, E. Isogai, and T. Yokochi for comments and advice.

Author Contributions

Conceived and designed the experiments: YS AN. Performed the experiments: YS SMRI JA YK MK YT HK SHo WS MO SHa AT. Analyzed the data: YS MK YT HK SHo MI TS MO SHa AT AN. Contributed reagents/materials/analysis tools: DM MY YN. Wrote the paper: YS AN.

References

1. Jacob F (1977) Evolution and tinkering. Science 196: 1161–1166.
2. Ohno S (1970) Evolution by gene duplication. New York, NY, Springer-Verlag.
3. Tautz D, Domazet-Loso T (2011) The evolutionary origin of orphan genes. Nat Rev Genet 12: 692–702.
4. Kaessmann H (2010) Origins, evolution, and phenotypic impact of new genes. Genome Res 20: 1313–1326.
5. Khalturin K, Hemmrich G, Fraune S, Augustin R, Bosch TC (2009) More than just orphans: are taxonomically-restricted genes important in evolution? Trends Genet 25: 404–413.
6. Carvunis AR, Rolland T, Wapinski I, Calderwood MA, Yildirim MA, et al. (2012) Proto-genes and de novo gene birth. Nature 487: 370–374.
7. Li D, Dong Y, Jiang Y, Jiang H, Cai J, et al. (2010) A de novo originated gene depresses budding yeast mating pathway and is repressed by the protein encoded by its antisense strand. Cell Res 20: 408–420.
8. Begun DJ, Lindfors HA, Thompson ME, Holloway AK (2006) Recently evolved genes identified from Drosophila yakuba and D. erecta accessory gland expressed sequence tags. Genetics 172: 1675–1681.
9. Begun DJ, Lindfors HA, Kern AD, Jones CD (2007) Evidence for de novo evolution of testis-expressed genes in the Drosophila yakuba/Drosophila erecta clade. Genetics 176: 1131–1137.
10. Cai J, Zhao R, Jiang H, Wang W (2008) De novo origination of a new protein-coding gene in Saccharomyces cerevisiae. Genetics 179: 487–496.
11. Chen ST, Cheng HC, Barbash DA, Yang HP (2007) Evolution of hydra, a recently evolved testis-expressed gene with nine alternative first exons in Drosophila melanogaster. PLoS Genet 3: e107.
12. Toll-Riera M, Bosch N, Bellora N, Castelo R, Armengol L, et al. (2009) Origin of primate orphan genes: a comparative genomics approach. Mol Biol Evol 26: 603–612.
13. Knowles DG, McLysaght A (2009) Recent de novo origin of human protein-coding genes. Genome Res 19: 1752–1759.
14. Li CY, Zhang Y, Wang Z, Cao C, Zhang PW, et al. (2010) A human-specific de novo protein-coding gene associated with human brain functions. PLoS Comput Biol 6: e1000734.
15. O'Bleness M, Searles VB, Varki A, Gagneux P, Sikela JM (2012) Evolution of genetic and genomic features unique to the human lineage. Nat Rev Genet 13: 853–866.
16. Wu DD, Irwin DM, Zhang YP (2011) De novo origin of human protein-coding genes. PLoS Genet 7: e1002379.
17. Xie C, Zhang YE, Chen JY, Liu CJ, Zhou WZ, et al. (2012) Hominoid-specific de novo protein-coding genes originating from long non-coding RNAs. PLoS Genet 8: e1002942.
18. Brodeur GM (2003) Neuroblastoma: biological insights into a clinical enigma. Nat Rev Cancer 3: 203–216.
19. Brodeur GM, Seeger RC, Schwab M, Varmus HE, Bishop JM (1984) Amplification of N-myc in untreated human neuroblastomas correlates with advanced disease stage. Science 224: 1121–1124.
20. Schwab M, Varmus HE, Bishop JM, Grzeschik KH, Naylor SL, et al. (1984) Chromosome localization in normal human cells and neuroblastomas of a gene related to c-myc. Nature 308: 288–291.
21. Weiss WA, Aldape K, Mohapatra G, Feuerstein BG, Bishop JM (1997) Targeted expression of MYCN causes neuroblastoma in transgenic mice. EMBO J 16: 2985–2995.
22. Cohn SL, London WB, Huang D, Katzenstein HM, Salwen HR, et al. (2000) MYCN expression is not prognostic of adverse outcome in advanced-stage neuroblastoma with nonamplified MYCN. J Clin Oncol 18: 3604–3613.
23. Nakagawara A, Arima M, Azar CG, Scavarda NJ, Brodeur GM (1992) Inverse relationship between trk expression and N-myc amplification in human neuroblastomas. Cancer Res 52: 1364–1368.
24. Armstrong BC, Krystal GW (1992) Isolation and characterization of complementary DNA for N-cym, a gene encoded by the DNA strand opposite to N-myc. Cell Growth Differ 3: 385–390.
25. Krystal GW, Armstrong BC, Battey JF (1990) N-myc mRNA forms an RNA-RNA duplex with endogenous antisense transcripts. Mol Cell Biol 10: 4180–4191.
26. Jacobs JF, van Bokhoven H, van Leeuwen FN, Hulsbergen-van de Kaa CA, de Vries IJ, et al. (2009) Regulation of MYCN expression in human neuroblastoma cells. BMC Cancer 9: 239.
27. Suenaga Y, Kaneko Y, Matsumoto D, Hossain MS, Ozaki T, et al. (2009) Positive auto-regulation of MYCN in human neuroblastoma. Biochem Biophys Res Commun 390: 21–26.
28. Gustafson WC, Weiss WA (2010) Myc proteins as therapeutic targets. Oncogene 29: 1249–1259.
29. Sjostrom SK, Finn G, Hahn WC, Rowitch DH, Kenney AM (2005) The Cdk1 complex plays a prime role in regulating N-myc phosphorylation and turnover in neural precursors. Dev Cell 9: 327–338.
30. Kang JH, Rychahou PG, Ishola TA, Qiao J, Evers BM, et al. (2006) MYCN silencing induces differentiation and apoptosis in human neuroblastoma cells. Biochem Biophys Res Commun 351:192–197.
31. Zhang HH, Lipovsky AI, Dibble CC, Sahin M, Manning BD (2006) S6K1 regulates GSK3 under conditions of mTOR-dependent feedback inhibition of Akt. Mol Cell 24: 185–197.
32. Chanthery YH, Gustafson WC, Itsara M, Persson A, Hackett CS, et al. (2012) Paracrine signaling through MYCN enhances tumor-vascular interactions in neuroblastoma. Sci Transl Med 4: 115ra113.
33. Schramm A, Köster J, Marschall T, Martin M, Schwermer M, et al. (2013) Next-generation RNA sequencing reveals differential expression of MYCN target genes and suggests the mTOR pathway as a promising therapy target in MYCN-amplified neuroblastoma. Int J Cancer 132:E106–115.
34. Johnsen JI, Segerström L, Orrego A, Elfman L, Henriksson M, et al. (2008) Inhibitors of mammalian target of rapamycin downregulate MYCN protein expression and inhibit neuroblastoma growth in vitro and in vivo. Oncogene 27: 2910–2922.

35. Yu F, Gao W, Yokochi T, Suenaga Y, Ando K, et al. (2013) RUNX3 interacts with MYCN and facilitates protein degradation in neuroblastoma. Oncogene [epub ahead of print]
36. Otto T, Horn S, Brockmann M, Eilers U, Schüttrumpf L, et al. (2009) Stabilization of N-Myc is a critical function of Aurora A in human neuroblastoma. Cancer Cell 15:67–78.
37. Berry T, Luther W, Bhatnagar N, Jamin Y, Poon E, et al. (2012) The ALK(F1174L) mutation potentiates the oncogenic activity of MYCN in neuroblastoma. Cancer Cell 22: 117–130.
38. Heukamp LC, Thor T, Schramm A, De Preter K, Kumps C, et al. (2012) Targeted expression of mutated ALK induces neuroblastoma in transgenic mice. Sci Transl Med 4: 141ra191.
39. Molenaar JJ, Domingo-Fernandez R, Ebus ME, Lindner S, Koster J, et al. (2012) LIN28B induces neuroblastoma and enhances MYCN levels via let-7 suppression. Nat Genet 44: 1199–1206.
40. Valentijn LJ, Koster J, Haneveld F, Aissa RA, van Sluis P, et al. (2012) Functional MYCN signature predicts outcome of neuroblastoma irrespective of MYCN amplification. Proc Natl Acad Sci U S A 109: 19190–19195.
41. Li Z, Tan F, Thiele CJ. (2007) Inactivation of glycogen synthase kinase-3beta contributes to brain-derived neutrophic factor/TrkB-induced resistance to chemotherapy in neuroblastoma cells. Mol Cancer Ther 6:3113–3121.
42. Kent WJ (2002) BLAT–the BLAST-like alignment tool. Genome Res 12: 656–664.
43. Blanchette M, Kent WJ, Riemer C, Elnitski L, Smit AF, et al. (2004) Aligning multiple genomic sequences with the threaded blockset aligner. Genome Res 14: 708–715.
44. Altschul SF, Madden TL, Schaffer AA, Zhang J, Zhang Z, et al. (1997) Gapped BLAST and PSI-BLAST: a new generation of protein database search programs. Nucleic Acids Res 25: 3389–3402.
45. Wang D, Zhang Y, Zhang Z, Zhu J, Yu J (2010) KaKs_Calculator 2.0: a toolkit incorporating gamma-series methods and sliding window strategies. Genomics Proteomics Bioinformatics 8: 77–80.
46. Ohira M, Oba S, Nakamura Y, Isogai E, Kaneko S, et al. (2005) Expression profiling using a tumor-specific cDNA microarray predicts the prognosis of intermediate risk neuroblastomas. Cancer Cell 7: 337–350.

European Journal of Cancer (2014) 50, 1555–1565

Available at www.sciencedirect.com

ScienceDirect

journal homepage: www.ejcancer.com

Novel 1p tumour suppressor Dnmt1-associated protein 1 regulates MYCN/ataxia telangiectasia mutated/p53 pathway

Yohko Yamaguchi [a], Hisanori Takenobu [a], Miki Ohira [b], Atsuko Nakazawa [c], Sayaka Yoshida [a], Nobuhiro Akita [a], Osamu Shimozato [a], Atsushi Iwama [d], Akira Nakagawara [e], Takehiko Kamijo [a,*]

[a] *Division of Biochemistry and Molecular Carcinogenesis, Chiba Cancer Center Research Institute, Japan*
[b] *Laboratory of Cancer Genomics, Chiba Cancer Center Research Institute, Japan*
[c] *Department of Pathology, National Center for Child Health and Development, Japan*
[d] *Department of Cellular and Molecular Medicine, Graduate School of Medicine, Chiba University, Chiba, Japan*
[e] *Division of Biochemistry and Innovative Cancer Therapeutics, Chiba Cancer Center Research Institute, Japan*

Available online 19 February 2014

KEYWORDS
DMAP1
ATM
p53
Neuroblastoma
MYCN

Abstract Neuroblastoma (NB) is a paediatric solid tumour which originates from sympathetic nervous tissues. Deletions in chromosome 1p are frequently found in unfavourable NBs and are correlated with v-myc avian myelocytomatosis viral oncogene neuroblastoma derived homolog (*MYCN*) amplification; however, it remains to be elucidated how the 1p loss contributes to MYCN-related oncogenic processes in NB. In this study, we identified the role of Dnmt1-associated protein 1 (DMAP1), coded on chromosome 1p34, in the processes.
We studied the expression and function of DMAP1 in NB and found that low-level expression of DMAP1 related to poor prognosis, unfavourable histology and 1p Loss of heterozygosity (LOH) of primary NB samples. Intriguingly, DMAP1 induced ataxia telangiectasia mutated (ATM) phosphorylation and focus formation in the presence of a DNA damage reagent, doxorubicin. By DMAP1 expression in NB and fibroblasts, p53 was activated in an ATM-dependent manner and p53-downstream pro-apoptotic Bcl-2 family molecules were induced at the mRNA level, resulting in p53-induced apoptotic death. *BAX* and $p21^{Cip1/Waf1}$ promoter activity dependent on p53 was clearly up-regulated by DMAP1. Further, MYCN transduction in *MYCN* single-copy NB cells accelerated doxorubicin (Doxo)-induced apoptotic cell death; MYCN is implicated in DMAP1 protein stabilisation and ATM phosphorylation in these situations. DMAP1 knockdown attenuated MYCN-dependent ATM phosphorylation and NB cell apoptosis. Together, DMAP1

* *Corresponding author:* Address: Division of Biochemistry and Molecular Carcinogenesis, Chiba Cancer Center Research Institute, 666-2 Nitona, Chuo-ku, Chiba 260-8717, Japan. Tel.: +81 43 264 5431; fax: +81 43 265 4459.
E-mail address: tkamijo@chiba-cc.jp (T. Kamijo).

http://dx.doi.org/10.1016/j.ejca.2014.01.023

appears to be a new candidate for a 1p tumour suppressor and its reduction contributes to NB tumourigenesis via inhibition of MYCN-related ATM/p53 pathway activation.

1. Introduction

Genetic and molecular analyses have indicated various types of deletions of the short arm of chromosome 1 (1p) in a broad range of human malignant tumours, including neuroblastoma (NB) and others [1–5]. It has been suggested that this genomic region harbours several tumour suppressor genes and that additive effects of loss of those tumour suppressors on tumourigenesis exist in several '1p loss malignant tumours'.

NB is the second most common paediatric solid malignant tumour derived from sympathetic nervous tissues. Extensive cytogenetic and molecular genetic studies have identified that genetic abnormalities, such as loss of the short arm of 1p, 11q and 14q; amplification of *MYCN*; and allelic gain of 11p and 17q, are frequently observed [1]. Deletion of the 1p region is highly correlated with both *MYCN* amplification and an adverse patient outcome, indicating the presence of several tumour suppressor genes (TSGs) within this region [6]. NB tumours with *MYCN* in a single copy had preferentially lost the 1p36 allele and these tumours also had a very distal commonly deleted region; in contrast, all *MYCN*-amplified NBs had larger 1p deletions, extending from the telomere to 1p31 [7]. The extent of deletion or LOH was identified in 184 primary NBs; in 80%, the 1p deletion extended from the telomere to 1p31 [8]. Given the tendency of large, hemizygous 1p deletions in *MYCN*-amplified NBs, alternative hypotheses for tumour suppression are: (1) an additional, *MYCN*-associated TSG in the 1p region; (2) suppression of TSG expression from a hemizygous allele due to epigenetic modifications except for imprinting, e.g. miRNAs and non-coding RNAs; (3) haplo-insufficiency-based suppression accounting for the rarity of 1p homozygous deletions [9].

Dnmt1-associated protein 1 (DMAP1) was originally identified as a molecule interacting with DNMT1 and was demonstrated to co-localise with PCNA and DNMT1 at DNA replication foci during the S phase [10]. Previously, we reported that Dmap1 participates in DNA repair and transformation of mouse embryonic fibroblasts (MEFs). Dmap1 was recruited to the damaged sites, formed complexes with γ-H2AX and directly interacted with Proliferating Cell Nuclear Antigen (Pcna); inhibition of this binding impaired the accumulation of the Pcna-Caf-1 complex at damaged sites and resulted in DNA breaks [11]. In addition, Penicud and Behrens reported that DMAP1 promotes ataxia telangiectasia mutated (ATM) recruitment and focus formation at damaged sites. These results suggest that DMAP1 is involved in the DNA damage response (DDR) [12]. Interestingly, DMAP1 gene is coded in 1p34 and the region that is frequently deleted in NB tumours with 1p LOH [8,9]. These results prompted us to study the expression level of DMAP1 in neuroblastoma samples and its functional role in tumourigenesis.

In the present report, for the first time, we found that DMAP1 is a novel 1p tumour suppressor and DMAP1 has an indispensable role in MYCN-related ATM/p53 pathway activation. Downregulation of DMAP1 seems to be a result of MYCN-induced stress and an important mechanism for NB tumourigenesis.

2. Materials and methods

2.1. Cell culture

Human NB cell lines were obtained from official cell banks (RIKEN Bioresource Cell Bank, Tohoku University Cell Resource Center, and the American Type Culture Collection) and were cultured in RPMI1640 or Dulbecco's modified Eagle's medium (Wako, Osaka, Japan) supplemented with 10% heat-inactivated foetal bovine serum (Invitrogen, Carlsbad, CA, United States of America (USA)) and 50 μg/ml penicillin/streptomycin (Sigma–Aldrich, St. Louis, MO, USA) in an incubator with humidified air at 37 °C with 5% CO_2. ATM kinase inhibitor, KU-55933 (Santa Cruz Biotechnology, Santa Cruz, CA, USA) was dissolved in DMSO to make stock solutions of 20 mM.

2.2. Lentiviral production and infection for over-expression and knockdown of genes

For the over-expression of mouse Dmap1 and human DMAP1, cDNAs were subcloned into lentiviral vector pHR-SIN-CSGW [13]. For shRNA-based knockdown experiments, pLKO.1 puromycin-based lentiviral vectors containing five sequence-verified shRNAs targeting human DMAP1 (RefSeq NM_019100.4, NM_001034024.1, NM_001034023.1) were obtained from the MISSION TRC-Hs 1.0 Human, shRNA library (Sigma–Aldrich). We checked DMAP1 knockdown by five lentivirus-produced shRNAs (clones: TRCN0000021744-21748) and used at least two shRNAs for experiments. Lentiviral production, infection and confirmation of infection efficiency were performed as described previously [13].

2.3. Antibodies

Antibodies against p53 (DO-1) and MYCN (rabbit polyclonal, C-19) were purchased from Santa Cruz Biotechnology. Antibodies against p53Ser15-P (rabbit

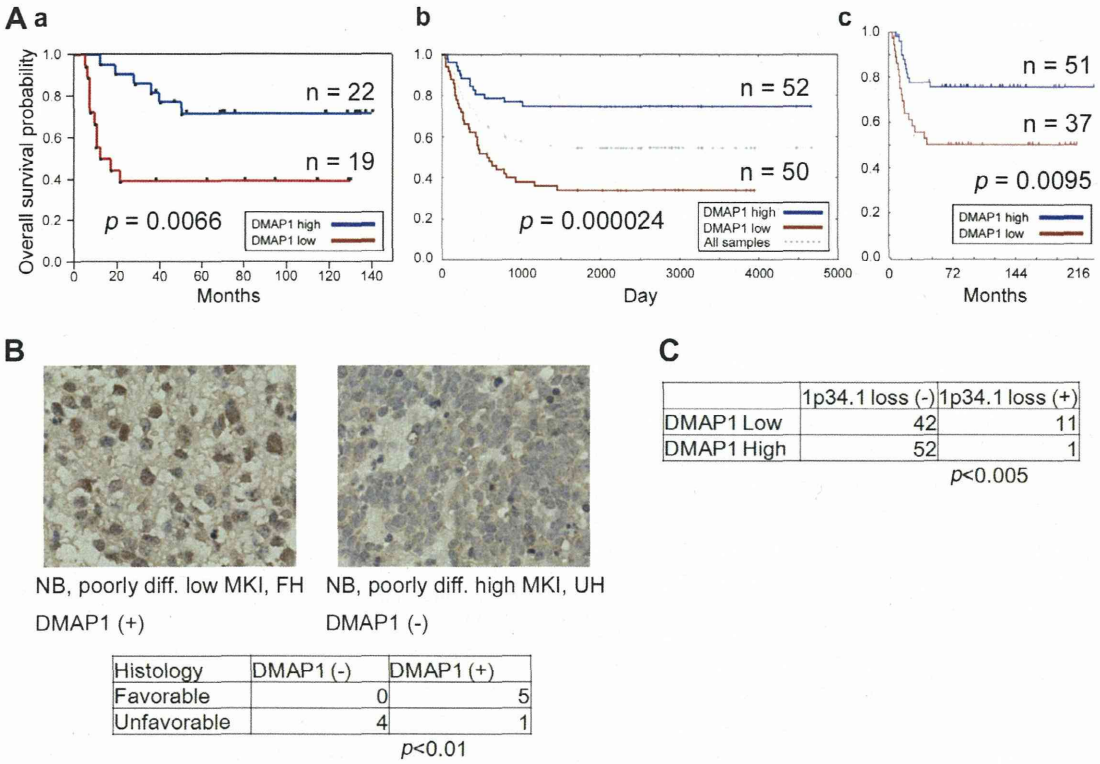

	1p34.1 loss (-)	1p34.1 loss (+)
DMAP1 Low	42	11
DMAP1 High	52	1

$p<0.005$

Histology	DMAP1 (-)	DMAP1 (+)
Favorable	0	5
Unfavorable	4	1

$p<0.01$

Fig. 1. Expression level of Dnmt1-associated protein 1 (DMAP1) in neuroblastoma (NB) samples and neuroblastoma cell lines. (A) Kaplan–Meier survival analysis of NB patients based on higher or lower expression levels of *DAMP1* (overall survival analysis) presented by microarray analysis in three individual cohorts. (Aa) Chiba Cancer Center Research Institute cohort ($n = 41$). Expression levels of *DMAP1* were separated into a high or low group based on the average expression. Statistical analysis was performed by the log-rank test. Corresponding p values are indicated. (Ab) Childrens Hospital Los Angeles cohort (http://pob.abcc.ncifcrf.gov/cgi-bin/JK), Neuroblastoma Prognosis Database-Seeger Lab dataset. $n = 102$. Expression levels of *DMAP1* on probe 224163_s_at were separated into a high or low group based on the median expression. (Ac) Academic Medical Center cohort R2 microarray analysis and visualisation platform (http://r2.amc.nl), Tumor Neuroblastoma public-Versteeg-88 dataset. $n = 88$. Expression levels of *DMAP1* on probe 224163_s_at were separated into a high or low group based on the expression cutoff value 118.0 according to the R2 algorithm. (B) Immunohistochemical staining for DMAP1 in NB. Statistical significance was determined by Fisher's exact probability test. MKI: Mitosis-karyorrhexis index. FH: favourable histology; UH: unfavourable histology. DMAP1 (+): DMAP1 high-expression tumour; DMAP1 (−): DMAP1 low-expression tumour. (C) 1p loss was studied by array CGH analysis. Expression status of *DMAP1* was quantified by quantitative polymerase chain reaction (qPCR) analysis and normalised by *GAPDH* expression. *DMAP1* high or low expression was determined by its median value. Fisher's exact probability test was applied to determine statistical significance.

polyclonal) and ATMSer1981-P (10H11. E12) were from Cell Signaling Technology (Danvers, MA, USA). Anti-ATM rabbit polyclonal antibody (Ab-3) was from Merck Millipore. Antibodies against β-Actin (rabbit polyclonal) and anti-FLAG (M2) were from Sigma–Aldrich. A mouse monoclonal anti-tubulin antibody was from Neomarkers Lab Vision (Fremont, CA, USA). Anti-DMAP1 rabbit polyclonal antibody (ab2848) was from Abcam (Cambridge, United Kingdom (UK)), anti-DMAP1 (2G12) was from Abnova (Taipei, Taiwan) and anti-human influenza hemagglutinin (HA) rabbit polyclonal was from MBL (Nagoya, Japan).

2.4. Statistical analysis

All data were tested statistically using the Welch test and Fisher's exact probability test. $p < 0.05$ was considered to indicate statistical significance. Kaplan–Meier survival curves were calculated, and survival distributions were compared using the log-rank test. Cox regression models were used to explore associations between *DMAP1* expression, age at diagnosis, tumour stage, *TrkA* expression, *MYCN* copy number, tumour origin, DNA ploidy, Shimada pathology and survival. Statistical significance was declared if $p < 0.05$. Statistical analysis was performed using JMP 8.0 (SAS Institute Inc., Cary, NC, USA).

Other methods are described in Supplementary information.

3. Results

3.1. Low expression level of DMAP1 correlated with unfavourable prognosis of NB patients

We examined the expression levels of *DMAP1* in NB samples by microarray analysis. Kaplan–Meier survival analysis showed that low *DMAP1* expression correlated

with the unfavourable prognosis of NB patients (Fig. 1Aa). Web-based microarray analysis and visualisation application for NB confirmed these results (Fig. 1Ab, c), and it was also shown by quantitative polymerase chain reaction (qPCR) (Suppl. Fig. S1Aa). Unfavourable NBs, which are classified by International Neuroblastoma Staging System (INSS) stage with *MYCN* copy number, also expressed low-level *DMAP1* (Suppl. Fig. S1B). Immunohistochemical analysis also showed low expression of *DMAP1* in unfavourable histology NB (Fig. 1B).

Next, the chromosome 1p status was analysed by array CGH to study the mechanism of *DMAP1* reduction in unfavourable NB (Fig. 1C). As a result, *DMAP1* reduction in unfavourable NB was significantly correlated with loss of its gene locus. DMAP1 mRNA levels were significantly lower in NB cell lines than in primary NB samples (Suppl. Fig. S1C). To further assess other possibilities for the suppression of *DMAP1* expression, bisulphite sequencing was carried out using five clinical samples and two cell lines of NB and *BMI1* knockdown to study epigenetic suppression by polycombs in NB cell lines; however, DNA methylation of the *DMAP1* promoter region and transcriptional suppression of *DMAP1* by *BMI1* were not found (data not shown). Next, univariate Cox regression was employed to examine the individual relationship of each variable to survival (Table 1). These variables were: *DMAP1* expression, age at diagnosis (>1 year old versus <1 year old), tumour stage (3 + 4 versus 1 + 2 + 4s), *TrkA* expression (low versus high), *MYCN* copy number (amplified versus non-amplified), origin (adrenal gland versus others), DNA ploidy (aneuploidy versus di-/tetraploidy) and Shimada pathology (favourable versus unfavourable), all of which were found statistically to be of prognostic importance. Additionally, multivariable Cox analysis demonstrated that *DMAP1* expression was an independent prognostic factor from tumour origin, stage and DNA ploidy. However, the analysis showed a correlation between *DMAP1* reduction and *MYCN* amplification (Table 1). These results suggested that *DMAP1* works as a tumour suppressor gene in NB and its expression levels strongly correlate with *MYCN* copy numbers.

Table 1
Correlation between Dnmt1-associated protein 1 (DMAP1) expression and other prognostic factors of neuroblastoma.

Terms	High DMAP1	Low DMAP1	*p*-Value
Age (years)			
⩽1.5	25	33	0.13
>1.5	31	23	
Tumour origin			
Adrenal	29	28	0.773
Others	26	28	
Stage			
1, 2, 4S	29	22	0.184
3, 4	27	34	
Shimada pathology			
Favourable	37	30	0.16
Unfavourable	12	18	
MYCN copy number			
Single	52	41	<0.01
Amplified	4	15	
TrkA expression			
High	32	28	0.507
Low	23	26	
DNA index			
Diploidy	22	27	0.186
Aneuploidy	28	20	

MYCN: Fisher's exact probability test, $\chi^2 = 7.669496321$, $p < 0.01$.

3.2. DMAP1 activated ATM and p53 with DNA damage

In our previous study, we observed that Dmap1 knockdown in MEFs leads to the failure of DNA repair, resulting in accumulated DNA damage [11]. These results prompted us to study the role of DMAP1 in DDR, including the ATM/p53 pathway. In response to DNA damage, ATM forms foci at double-stranded DNA break (DSB) sites and undergoes self-phosphorylation at serine 1981 to enhance its kinase activity. The activated ATM phosphorylates p53 at serine 15, which in turn induces p53-downstream effectors, leading to the inhibition of cell cycle progression or apoptotic cell death [14]. For DNA damage induction, we chose doxorubicin (Doxo) at 0.5 μg/ml concentration to assess the effect on NB cells according to the results of the analysis of peak plasma concentrations of doxorubicin [15].

We expressed DMAP1 in p53-wild type NB cells and found that ATMSer1981 phosphorylation increased for up to 6 h after Doxo treatment, and p53Ser15 phosphorylation was up-regulated subsequently (Fig. 2A). We also confirmed DMAP1-related p53Ser15 phosphorylation in human fibroblasts (Fig. 2B).

Next, SH-SY5Y cells, which express rather higher DMAP1 than other NB cell lines (Suppl. Fig. S1D), were infected with shDMAP1-expressing virus and treated with Doxo. Knockdown of DMAP1 resulted in downregulation of ATM and p53 phosphorylation (Fig. 2C). We then evaluated the focus formation of ATM. It was significantly suppressed 1.0 h but not 1.5–2.5 h after Doxo treatment by DMAP1 knockdown (Fig. 2D), suggesting that DMAP1 is required for efficient focus formation of ATM in the early stage of DDR.

3.3. DMAP1 activated p53 by ATM and induced transcription of p53-downstream genes

To examine whether p53 phosphorylation promoted by DMAP1 is dependent on ATM activity, we used an

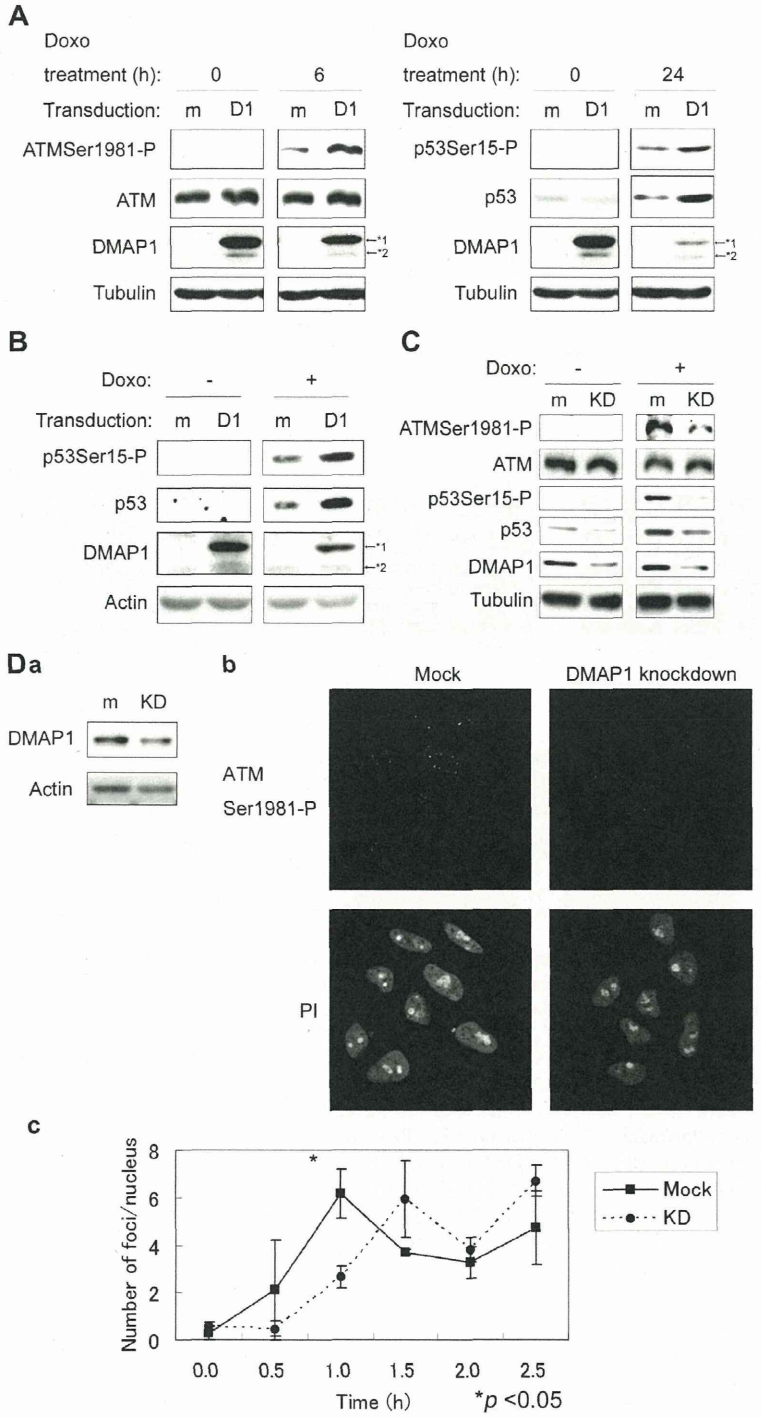

Fig. 2. Dnmt1-associated protein 1 (DMAP1) promoted focus formation of ataxia telangiectasia mutated (ATM) and activated ATM under doxorubicin (Doxo) treatment. (A) Phosphorylation status of ATMSer1981 and p53Ser15 in DMAP1 over-expressing cells. SK-N-SH cells were transduced with human influenza hemagglutinin (HA)-tagged DMAP1 and treated with Doxo for the indicated time period. The cells were subjected to sodium dodecyl sulphate–polyacrylamide gel electrophoresis (SDS–PAGE) and Western blot analysis. (B) Phosphorylation of p53Ser15 by DMAP1 in human fibroblasts (hfb). Hfb were transduced with HA-tagged DMAP1 and treated with Doxo for 24 h to confirm phosphorylation of p53 by Western blot analysis. (C) Phosphorylation status of ATMSer1981 in DMAP1 knocked-down cells. SH-SY5Y cells were infected with shDMAP1-expressing virus and treated with Doxo for 1 h. The cells were subjected to SDS–PAGE and Western blot analysis. (D) Focus formation of ATM in DMAP1 knocked-down cells. SH-SY5Y cells were infected with shDMAP1-expressing virus and treated with Doxo for the indicated time period, followed by SDS–PAGE, Western blot analysis (Da) and immunocytochemistry (ICC, Db). In ICC, cells were stained with anti-ATMSer1981-P and propidium iodide (PI). (Dc) Number of ATM foci was counted using the colony counting tool in Image Quant TL. Error bars represent S.D. obtained from triplicate samples. Data were analysed using the Welch test. Data are representative of three independent experiments. (A–D), m: mock, D1: DMAP1, KD: DMAP1 knockdown; *1: HA-DMAP1, *2: Endogenous DMAP1.

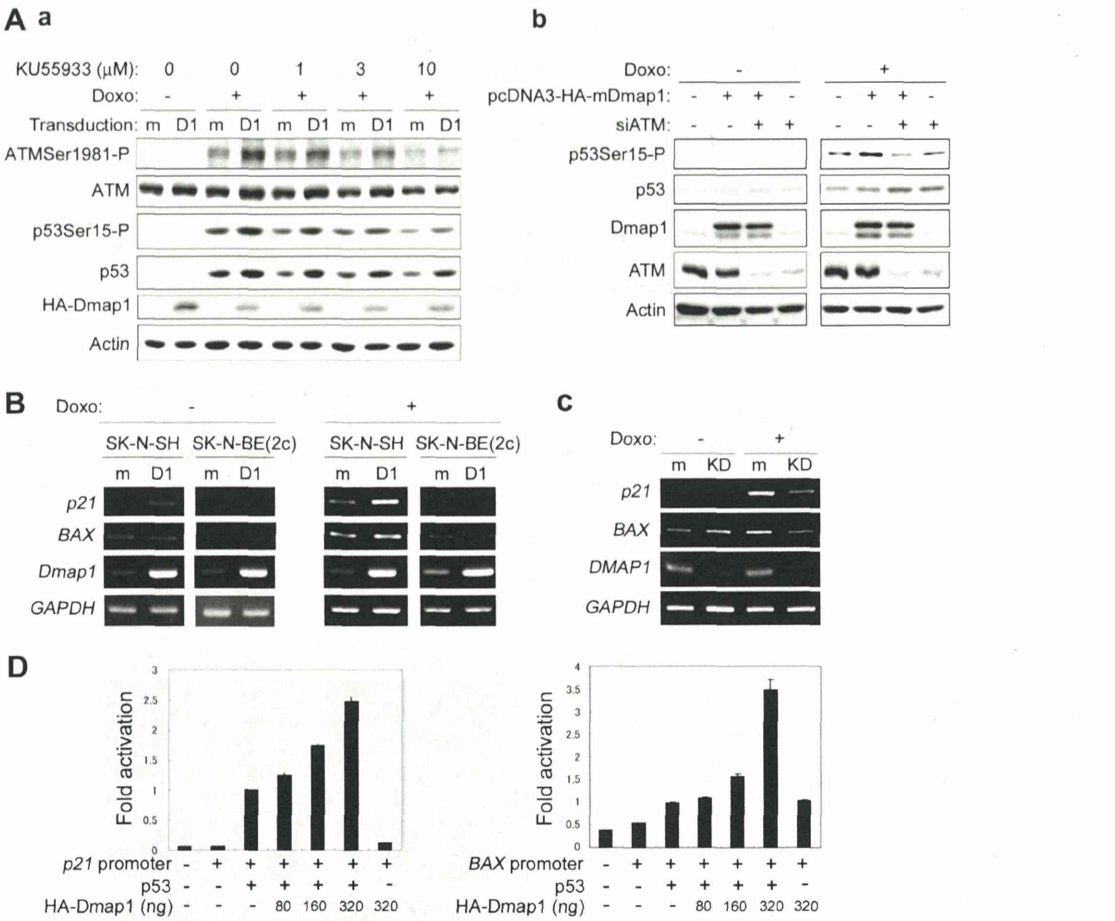

Fig. 3. Dnmt1-associated protein 1 (DMAP1) activated p53 via ataxia telangiectasia mutated (ATM). (A) Phosphorylation of p53Ser15 by Dmap1 thorough ATM activation. (Aa) SK-N-SH cells were infected with HA-tagged Dmap1-expressing virus and pre-treated with KU-55933. One hour after KU-55933 addition, cells were treated with doxorubicin (Doxo) for 12 h and subjected to sodium dodecyl sulphate–polyacrylamide gel electrophoresis (SDS–PAGE) and Western blot analysis. (Ab) SK-N-SH cells were transfected with *ATM* siRNA (sequence: 5′-AACATACTACTCAAAGACATT-3′, Sigma–Aldrich, St. Louis, MO, USA). or control siRNA (ON-TARGETplus Non-targeting siRNA #1, Thermo Fisher Scientific, Lafayette, CO, USA). Transfection of siRNA was performed according to a previous report (16). Forty-eight hours after forward transfection, the cells were treated with 0.3 μg/ml Doxo for 1 h and subjected to Western blot. m: mock, D1: Dmap1. (B, C) Semi-quantitative Reverse Transcription Polymerase Chain Reaction (RT-PCR) of p53-target genes in *Dmap1* over-expressing cells (B) and in DMAP1 knocked-down SH-SY5Y cells (C). m: mock, D1: Dmap1, KD: DMAP1 knockdown. (D) Luciferase reporter assay analysis of $p21^{Cip1/Waf1}$ and *BAX* promoter activity in H1299 cells. Increasing amount of pcDNA3-HA-Dmap1, constant amount of pcDNA 3-p53, Renilla luciferase reporter plasmid (pRL-TK) and luciferase reporter plasmid with p53 responsive elements were transfected, and luciferase activity was studied. Data are representative of three independent experiments ($n = 3$).

ATM-specific ATP-competitive inhibitor KU-55933. KU-55933 abrogated the Dmap1-induced phosphorylation of ATM and p53, indicating ATM dependency of Dmap1-related p53 phosphorylation (Fig. 3Aa). ATM knockdown further represented ATM-dependent p53Ser15 phosphorylation by DMAP1 (Fig. 3Ab). Downstream target genes of p53, such as $p21^{Cip1/Waf1}$ and *BAX*, were induced by Dmap1 in the presence or absence of Doxo in *p53*-wt SK-N-SH cells but were not induced in *p53*-mutated SK-N-BE(2c) cells (Fig. 3B). Knockdown of DMAP1 reduced p53 accumulation (Fig. 2C) and transcription of the downstream $p21^{Cip1/Waf1}$ and *BAX* in a Doxo-dependent manner (Fig. 3C). Transcription of *NOXA*, the pro-apoptotic Bcl-2 family molecule, which was previously shown to be a critical molecule in p53-related damage-induced NB cell death [16], was also upregulated by DMAP1 (Suppl. Fig. S2A). DMAP1-promoted upregulation of $p21^{Cip1/Waf1}$ and *BAX* promoter activity, which was mediated by p53, was confirmed by a luciferase reporter assay of *p53*-null H1299 cells (Fig. 3D).

3.4. DMAP1 acts as a tumour suppressor via p53 activation in NB cells

We examined the functional role of DMAP1 and its p53 dependency in NB cells. DMAP1 enhanced cell cycle arrest and apoptosis induced by Doxo in a

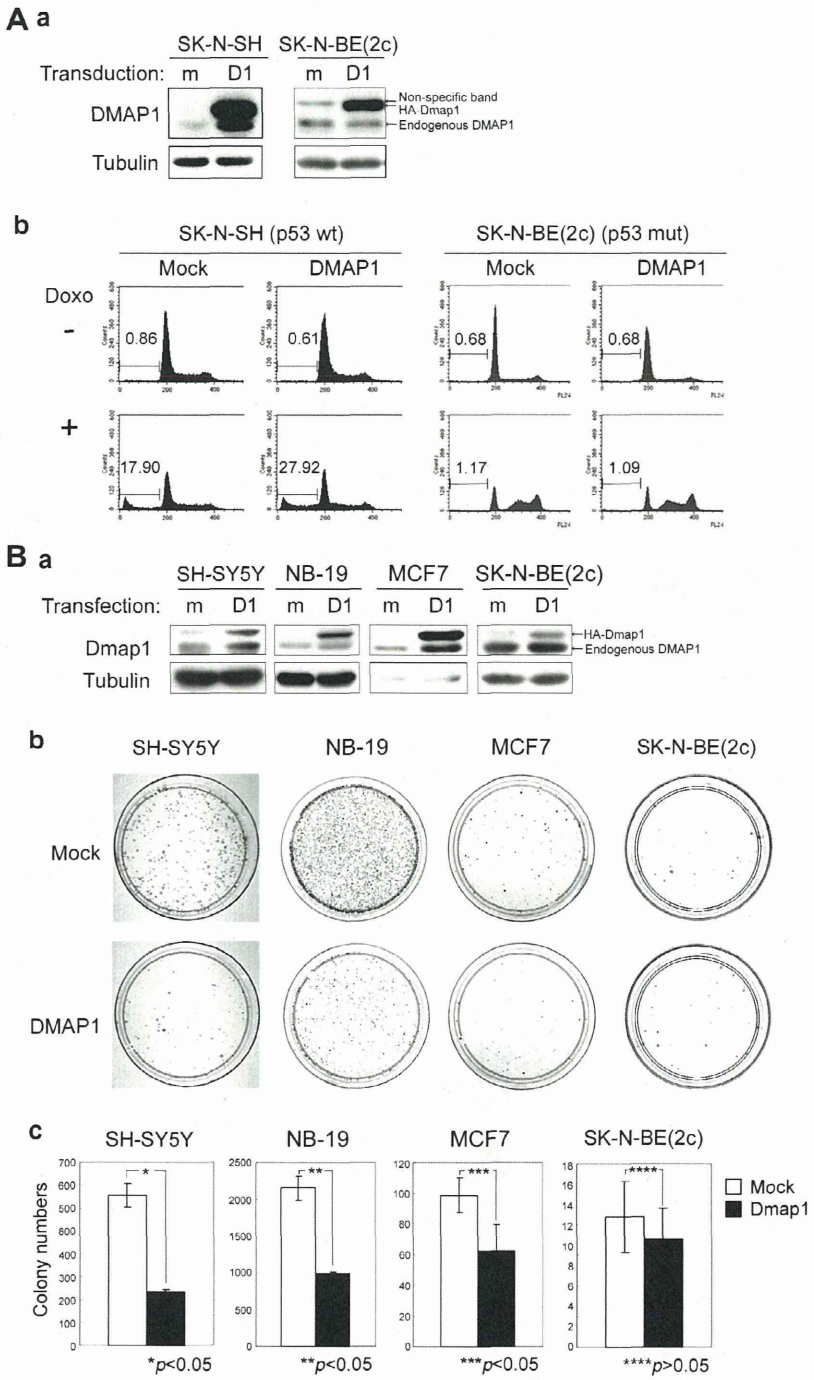

Fig. 4. Dnmt1-associated protein 1 (DMAP1) acts as a tumour suppressor via p53 activation in NB cells. (A) Dmap1-transduced NB cells were treated with doxorubicin (Doxo) and subjected to Western blot (Aa) and cell cycle analysis by flow cytometry (Ab). Numbers in histogram indicate % of subG0/G1 population. (B) Colony formation assay in Dmap1 over-expressing cells. Cells were transfected with pcDNA3-heteroduplex analysis (HA)-Dmap1 and subjected to Western blot (Ba) and selected with 400 μg/ml G418 for SH-SY5Y cells, 500 μg/ml G418 for NB-19 cells, 800 μg/ml G418 for MCF7 cells and 800 μg/ml G418 for SK-N-BE(2c) cells, for 2 weeks. (Bb) Colonies were stained with May-Grünwald's Eosin Methylene Blue Solution (Wako, Osaka, Japan) and Giemsa's solution (Merk Japan, Tokyo, Japan). (Bc) Number of colonies was counted using the colony counting tool in Image Quant TL. Error bars represent S.D. (A–B), m: mock, D1: Dmap1.

p53-dependent manner (Fig. 4A and Suppl. Fig. S2B). SH-SY5Y cells, NB-19 cells and breast cancer-derived MCF7 cells harbouring wild-type p53 were transfected with pcDNA3-HA-Dmap1 and selected with G418 for two weeks. As shown in Fig. 4B, Dmap1 significantly suppressed colony formation in these cells. These results suggested that DMAP1 acts as a tumour suppressor via p53 activation in NB cells.

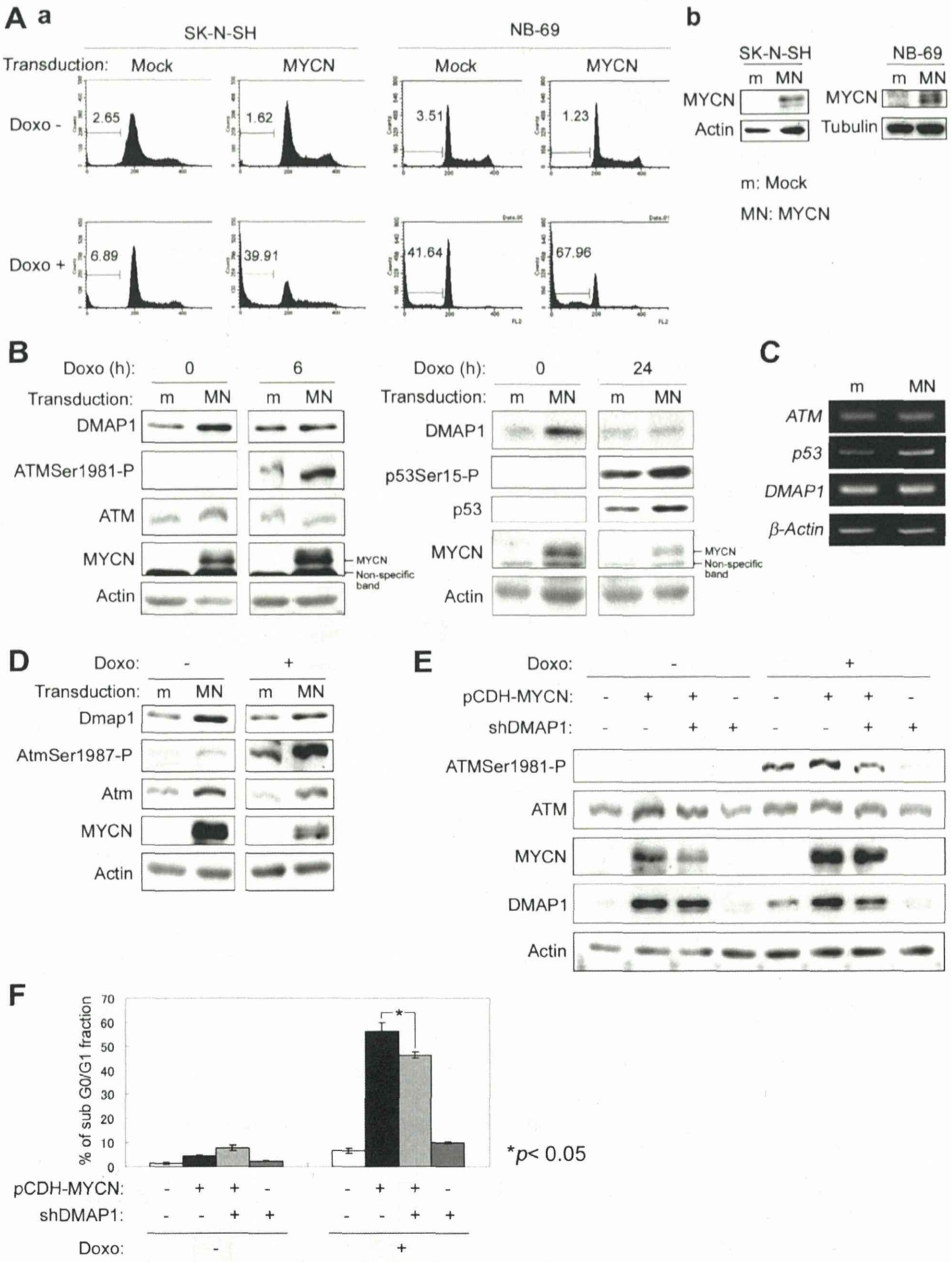

Fig. 5. MYCN promoted doxorubicin (Doxo)-induced apoptosis and ataxia telangiectasia mutated (ATM)/p53 activation. Cells were transduced with pCDH-MYCN and subjected to analysis as follows. (Aa) Cell cycle analysis [(Ab) protein expression was confirmed by Western blotting in left panel], (B) Western blot analysis and (C) semi-quantitative RT-PCR of MYCN over-expressing and Doxo-treated NB cells. Numbers in histogram indicate% of subG0/G1 population. (D) Activation of Atm/p53 pathway by MYCN in NIH3T3 cells. Cells were collected 12 h after Doxo treatment and subjected to Western blot analysis. (E, F) MYCN over-expression and/or Dnmt1-associated protein 1 (DMAP1) knockdown were performed as indicated in SK-N-SH cells. Cells were collected for Western blot analysis of ATMSer1981-P (E) and sub G0/G1 analysis (F) 6 h after Doxo treatment. (A–D) m: mock, MN: MYCN.

3.5. DMAP1 was implicated in MYCN-induced ATM activation

Given that *MYCN* amplification correlated with a low level of DMAP1 and that MYCN regulates the ATM/p53 pathway [17], we studied the DMAP1/ATM/p53 pathway in *MYCN*-transduced cells. As reported [18], exogenous MYCN promoted apoptosis in *MYCN* single-copy and *p53* wild type SK-N-SH cells and NB-69 cells (Fig. 5A) and activation of ATM/p53 under Doxo treatment in SK-N-SH cells (Fig. 5B left: 6 h after, right: 24 h after). Interestingly, the protein amount of DMAP1 was upregulated by MYCN although *DMAP1* mRNA was not increased (Fig. 5B, C).

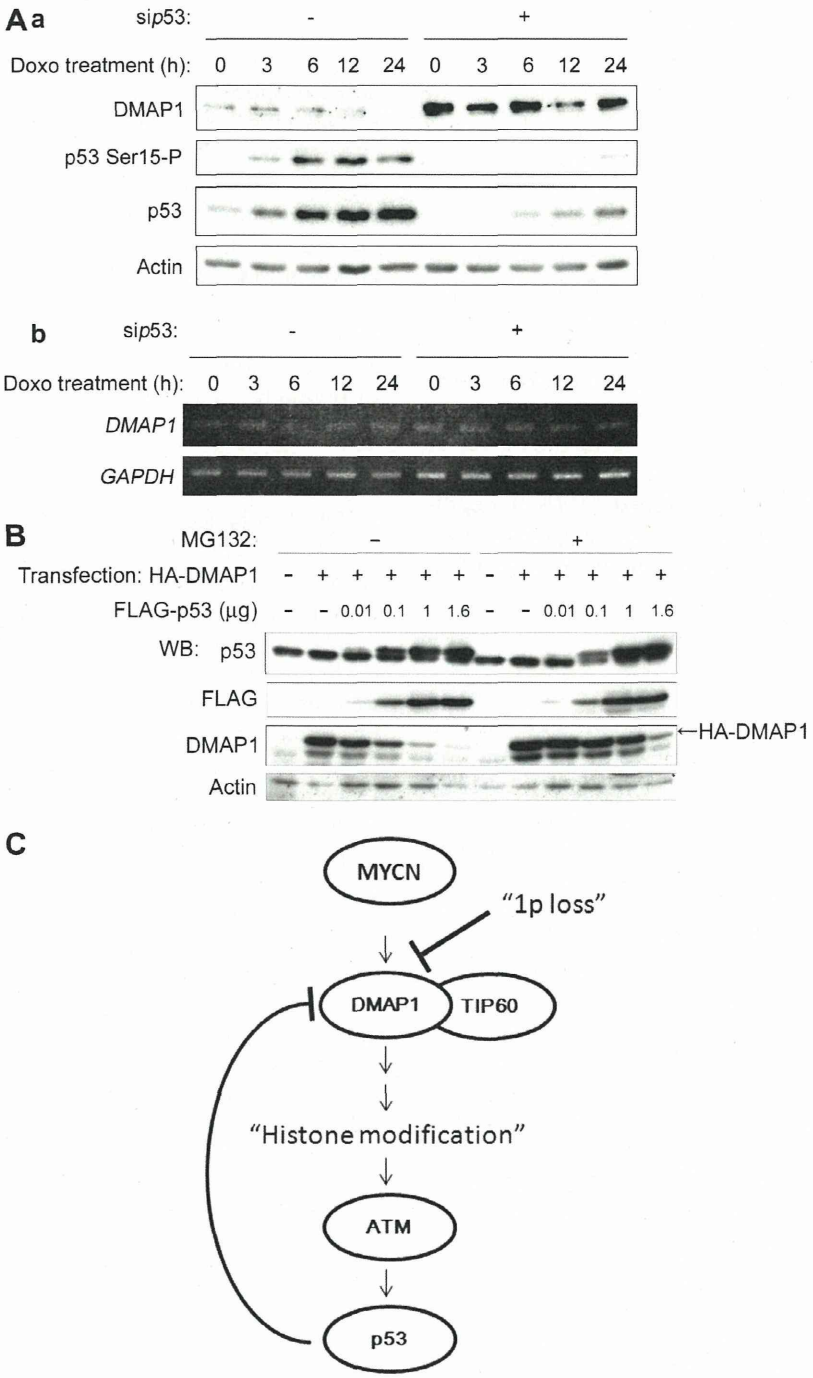

Fig. 6. Dnmt1-associated protein 1 (DMAP1) degradation by p53. (A) DMAP1 expression in p53 knocked-down cells. SK-N-SH cells harbouring wt-p53 were transfected with *p53* siRNA (ON-TARGETplus Duplex J-003329-14-0005, Human Tp53; Thermo Fisher Scientific, Lafayette, CO, USA) or control siRNA (Silencer_Negative Control #1 siRNA; Ambion Inc., Austin, TX, USA). Transfection of siRNA was performed according to a previous report (16). Forty-eight hours after forward transfection, the cells were treated with 0.3 μg/ml doxorubicin (Doxo) for the indicated time periods and subjected to Western blotting (Aa)/semi-quantitative RT-PCR (Ab). (B) Western blot analysis of Dmap1 degradation by p53 in combination with MG132 treatment. 293T cells were transfected with a constant amount of pcDNA3-heteroduplex analysis (HA)-tagged Dmap1 and increasing amounts of pcDNA3-FLAG-tagged p53 and then treated with 2 μM MG132 for 24 h. (C) MYCN/DMAP1/ataxia telangiectasia mutated (ATM)/p53 pathway regulates neuroblastoma cell death.

These phenomena were confirmed in *MYCN*-single copy, p53 wild-type NIH3T3 fibroblasts (Fig. 5D). Further, DMAP1 knockdown reduced the phosphorylation of ATM (Fig. 5E) and Doxo-induced apoptosis

(Fig. 5F), which were up-regulated by MYCN, indicating that DMAP1 was implicated in MYCN-induced ATM/p53 activation and apoptosis.

3.6. Negative feedback regulation of DMAP1 by p53

In MYCN-related ATM/p53 pathway activation, we found that DMAP1 protein was reduced, accompanied with p53 activation (Fig. 5B) and this DMAP1 reduction was also observed in DMAP1-tranduced cells after p53 activation by Doxo (Figs. 2A, B and 3A). To examine whether p53 reduces DMAP1, we knocked down p53 in NB cells (Fig. 6A). DMAP1 protein was clearly increased by p53 knockdown, but the mRNA level of DMAP1 was not affected. Proteasome inhibitor, MG132 treatment effectively inhibited DMAP1 degradation by p53 expression (Fig. 6B), suggesting that p53 promotes DMAP1 degradation in an ubiquitin–proteasome system-dependent manner.

4. Discussion

The proto-oncogenes *MYC* and *MYCN* have a pivotal function in growth control, differentiation and apoptosis and are among the most frequently affected genes in human malignant tumours; they are overexpressed in a large percentage of human tumours [19,20]. Transformation by Myc proteins requires concomitant inhibition of apoptosis by inactivation of apoptosis-inducing pathway genes [21]. One of the *MYC* oncogene product-related apoptotic pathways is involved in DDR [18]. Recent studies have clarified the relevant pathways regulating MYC-induced DDR, leading to the identification of ATM, TIP60 and WIP1 as mediators of this response [22]. Once ATM was activated by DNA damage, both p53 and proteins that interact with p53, MDM2 and Chk2 were phosphorylated by ATM, which in turn transactivated the p53-downstream effectors, leading to the inhibition of cell cycle progression or apoptotic cell death [23].

Regarding MYC/MYCN-related ATM regulation, this over-expression causes DNA damage *in vivo* and the ATM-dependent response to this damage is critical for p53 activation, apoptosis and the suppression of tumour development [22,24,25]. These findings suggested that MYC/MYCN expression induces ATM/p53 pathway activation by the related cellular stresses and subsequent inactivation of ATM will produce advantages for the tumourigenesis of MYC/MYCN-deregulated tumours. However, the occurrence of NB in ataxia-telangiectasia patients and ATM mutation in NB cells have not been reported to our knowledge, and mutations of p53 have been reported in <2% of NB [26,27], suggesting that functional inactivation of the pathway by other molecules seems to occur in NB tumours.

In the present study, we found that MYCN expression in *MYCN* single-copy cells increased DMAP1 and Doxo-induced apoptotic cell death (Fig. 5). DMAP1 induced ATMSer1981 phosphorylation and its focus formation in the presence of Doxo (Figs. 2 and 3A). By DMAP1 expression, p53Ser15 phosphorylation was induced in an ATM-dependent manner. In NB tumour samples, low expression of DMAP1 was related to poor prognosis, unfavourable histology, *MYCN* amplification and 1p LOH (Fig. 1, Table 1, Suppl. Fig. S1), suggesting that DMAP1 downregulation is required for NB tumourigenesis, especially under MYCN-induced cellular stress. Intriguingly, we observed negative feedback for degrading DMAP1, suggesting another DMAP1 downregulation mechanism in NB tumourigenesis (Fig. 6).

Recently, Penicud and Behrens reported that DMAP1 enhances Histone Acetyl Transferase (HAT) activity of TIP60 and promotes ATM auto-phosphorylation [12]. Depleting DMAP1 reduced ATM phosphorylation a few minutes after irradiation, but at later time points, it had no effect on ATM activation, as we previously reported [11]. Consistent with these observations, we found that DMAP1 knockdown delayed ATM focus formation and that the delay of ATM activation attenuated p53 phosphorylation and stabilisation. (Fig. 2C, D). These results indicate that DMAP1 regulates the efficient recruitment of ATM to the site of DNA breaks and this regulation is required for subsequent Doxo-induced p53-dependent cell death in NBs.

Taken together, we found that DMAP1 is a novel molecule of 1p tumour suppressors and has a role in ATM/p53 activation induced by MYCN-related cellular stresses (Fig. 6C). DMAP1 might be a new molecular target of MYCN-amplified NB treatment.

Conflict of interest statement

None declared.

Acknowledgements

We would like to thank Ms. Kumiko Sakurai and Dr. Masamitsu Negishi for technical help, and Daniel Mrozek, Medical English Service, for editorial assistance. *Grant Support:* This work was supported in part by a grant-in-aid from the National Cancer Center Research and Development Fund (4), a grant-in-aid from the Ministry of Health, Labor, and Welfare for Third Term Comprehensive Control Research for Cancer, and a Grant-in-Aid for Scientific Research (B) (24390269).

Appendix A. Supplementary data

Supplementary data associated with this article can be found, in the online version, at http://dx.doi.org/10.1016/j.ejca.2014.01.023.

References

[1] Brodeur GM. Neuroblastoma: biological insights into a clinical enigma. Nat Rev Cancer 2003;3:203–16.

[2] Praml C, Finke LH, Herfarth C, Schlag P, Schwab M, Amler L. Deletion mapping defines different regions in 1p34.2-pter that may harbor genetic information related to human colorectal cancer. Oncogene 1995;11:1357–62.

[3] Nagai H, Negrini M, Carter SL, et al. Detection and cloning of a common region of loss of heterozygosity at chromosome 1p in breast cancer. Cancer Res 1995;55:1752–7.

[4] Smith JS, Perry A, Borell TJ, et al. Alterations of chromosome arms 1p and 19q as predictors of survival in oligodendrogliomas, astrocytomas, and mixed oligoastrocytomas. J Clin Oncol 2000;18:636–45.

[5] Yang J, Du X, Lazar AJ, et al. Genetic aberrations of gastrointestinal stromal tumors. Cancer 2008;113:1532–43.

[6] Maris JM, Weiss MJ, Guo C, et al. Loss of heterozygosity at 1p36 independently predicts for disease progression but not decreased overall survival probability in neuroblastoma patients: a Children's Cancer Group study. J Clin Oncol 2000;18:1888–99.

[7] Martinsson T, Sjöberg RM, Hedborg F, Kogner P. Deletion of chromosome 1p loci and microsatellite instability in neuroblastomas analyzed with short-tandem repeat polymorphisms. Cancer Res 1995;55:5681–6.

[8] White PS, Thompson PM, Gotoh T, et al. Definition and characterization of a region of 1p36.3 consistently deleted in neuroblastoma. Oncogene 2005;24:2684–94.

[9] Hogarty MD, Winter CL, Liu X, et al. No evidence for the presence of an imprinted neuroblastoma suppressor gene within chromosome sub-band 1p36.3. Cancer Res 2002;62:6481–4.

[10] Rountree MR, Bachman KE, Baylin SB. DNMT1 binds HDAC2 and a new co-repressor, DMAP1, to form a complex at replication foci. Nat Genet 2000;25:269–77.

[11] Negishi M, Chiba T, Saraya A, Miyagi S, Iwama A. Dmap1 plays an essential role in the maintenance of genome integrity through the DNA repair process. Genes Cells 2009;14:1347–57.

[12] Penicud K, Behrens A. DMAP1 is an essential regulator of ATM activity and function. Oncogene 2014;33:525–31.

[13] Takenobu H, Shimozato O, Nakamura T, et al. CD133 suppresses neuroblastoma cell differentiation via signal pathway modification. Oncogene 2011;30:97–105.

[14] Lavin MF. Ataxia-telangiectasia: from a rare disorder to a paradigm for cell signalling and cancer. Nat Rev Mol Cell Biol 2008;9:759–69.

[15] James HD. Topoisomerase II inhibitors: anthracyclines. In: Chabner BA, Longo DL, editors. Cancer chemotherapy and biotherapy: principles and practice. Philadelphia: Lippincott Williams & Wilkins, a Wolters Kluwer Business; 2011. p. 356–91.

[16] Shi Y, Takenobu H, Kurata K, et al. HDM2 impairs Noxa transcription and affects apoptotic cell death in a p53/p73-dependent manner in neuroblastoma. Eur J Cancer 2010;46:2324–34.

[17] Hu H, Du L, Nagabayashi G, Seeger RC, Gatti RA. ATM is down-regulated by N-Myc-regulated microRNA-421. Proc Natl Acad Sci U S A 2010;107:1506–11.

[18] Fulda S, Lutz W, Schwab M, Debatin KM. MycN sensitizes neuroblastoma cells for drug-induced apoptosis. Oncogene 1999;18:1479–86.

[19] Evan GI, Littlewood TD. The role of c-myc in cell growth. Curr Opin Genet Dev 1993;3:44–9.

[20] Schwab M, Alitalo K, Klempnauer KH, et al. Amplified DNA with limited homology to myc cellular oncogene is shared by human neuroblastoma cell lines and a neuroblastoma tumour. Nature 1983;305:245–8.

[21] Gustafson WC, Weiss WA. Myc proteins as therapeutic targets. Oncogene 2010;29:1249–59.

[22] Campaner S, Amati B. Two sides of the Myc-induced DNA damage response: from tumor suppression to tumor maintenance. Cell Div 2012;7:6.

[23] Derheimer FA, Kastan MB. Multiple roles of ATM in monitoring and maintaining DNA integrity. FEBS Lett 2010;584:3675–81.

[24] Petroni M, Veschi V, Prodosmo A, et al. MYCN sensitizes human neuroblastoma to apoptosis by HIPK2 activation through a DNA damage response. Mol Cancer Res 2011;9:67–77.

[25] Swift M, Reitnauer PJ, Morrell D, Chase CL. Breast and other cancers in families with ataxia-telangiectasia. N Engl J Med 1987;316:1289–94.

[26] Vogan K, Bernstein M, Leclerc JM, Brisson L, Brossard J, Brodeur GM, et al. Absence of p53 gene mutations in primary neuroblastomas. Cancer Res 1993;53:5269–73.

[27] Tweddle DA, Malcolm AJ, Bown N, Pearson AD, Lunec J. Evidence for the development of p53 mutations after cytotoxic therapy in a neuroblastoma cell line. Cancer Res 2001;61:8–13, http://cancerres.aacrjournals.org/content/61/1/8.long.

Biochemical and Biophysical Research Communications 453 (2014) 86–93

Contents lists available at ScienceDirect

Biochemical and Biophysical Research Communications

journal homepage: www.elsevier.com/locate/ybbrc

Intracellular fragment of NLRR3 (NLRR3-ICD) stimulates ATRA-dependent neuroblastoma differentiation

Jesmin Akter [a], Atsushi Takatori [b,*], Md. Sazzadul Islam [a], Atsuko Nakazawa [c], Toshinori Ozaki [d,*], Hiroki Nagase [b], Akira Nakagawara [e]

[a] Laboratory of Innovative Cancer Therapeutics, Chiba Cancer Center Research Institute, Chiba 260-8717, Japan
[b] Laboratory of Cancer Genetics, Chiba Cancer Center Research Institute, Chiba 260-8717, Japan
[c] Department of Pathology, National Center for Child Health and Development, Tokyo, Japan
[d] Laboratory of DNA Damage Signaling, Chiba Cancer Center Research Institute, Chiba 260-8717, Japan
[e] Saga Medical Centre, 840-8571, Japan

ARTICLE INFO

Article history:
Received 13 September 2014
Available online 23 September 2014

Keywords:
ATRA
Differentiation
Neuroblastoma
NLRR3
Secretase

ABSTRACT

We have previously identified neuronal leucine-rich repeat protein-3 (NLRR3) gene which is preferentially expressed in favorable human neuroblastomas as compared with unfavorable ones. In this study, we have found for the first time that NLRR3 is proteolytically processed by secretases and its intracellular domain (NLRR3-ICD) is then released to translocate into cell nucleus during ATRA-mediated neuroblastoma differentiation. According to our present observations, NLRR3-ICD was induced to accumulate in cell nucleus of neuroblastoma SH-SY5Y cells following ATRA treatment. Since the proteolytic cleavage of NLRR3 was blocked by α- or γ-secretase inhibitor, it is likely that NLRR3-ICD is produced through the secretase-mediated processing of NLRR3. Intriguingly, forced expression of NLRR3-ICD in neuroblastoma SK-N-BE cells significantly suppressed their proliferation as examined by a live-cell imaging system and colony formation assay. Similar results were also obtained in neuroblastoma TGW cells. Furthermore, overexpression of NLRR3-ICD stimulated ATRA-dependent neurite elongation in SK-N-BE cells. Together, our present results strongly suggest that NLRR3-ICD produced by the secretase-mediated proteolytic processing of NLRR3 plays a crucial role in ATRA-mediated neuronal differentiation, and provide a clue to develop a novel therapeutic strategy against aggressive neuroblastomas.

1. Introduction

Neuroblastoma which originates from the sympathetic nervous system during embryogenesis, is the most common extra cranial solid tumor in children, accounting for 15% of childhood cancer deaths [1]. Neuroblastoma is highly heterogeneous, and thus characterized by a wide variety of its clinical behaviors, from spontaneous regression to aggressive progression. For example, tumors found in infants less than 1 year of age frequently regress through the spontaneous differentiation and/or apoptosis, resulting in a favorable prognosis [2]. It has been shown that neuroblastoma cells with better prognosis are often found to express various prognostic markers indicative of cell differentiation, such as *HNK-1* or *TrkA* [3,4]. On the other hand, around 40% of the patients diagnosed with neuroblastoma are included in the high-risk category based on prognostic indicators such as age at diagnosis, stage, tumor histology, proto-oncogene *MYCN* status, and DNA ploidy [5,6]. Among them, the poor clinical outcome and aggressive tumor phenotype of high-risk neuroblastoma strongly correlate with the amplification of *MYCN* and enhanced tumor angiogenesis [7]. Although patients with the high-risk tumors usually have a good immediate response to the standard treatment, the majority of them frequently acquire resistance to the therapy with fatal outcome [1]. Therefore, a novel strategy to treat these advanced tumors is highly required.

Intriguingly, neuroblastoma cells display the similar characteristics to undifferentiated cells [8], indicating that the tumorigenesis of neuroblastoma results from defect in differentiation of embryonic neural crest progenitor cells [9]. With this in mind, a growing body of evidence strongly suggests that neuroblastoma cells have an ability to differentiate into mature cells and can be

* Corresponding authors at: Laboratory of Cancer Genetics, Chiba Cancer Center Research Institute, 666-2 Nitona, Chuoh-ku, Chiba 260-8717, Japan. Fax: +81 43 265 4459 (A. Takatori). Laboratory of DNA Damage Signaling, Chiba Cancer Center Research Institute, 666-2 Nitona, Chuoh-ku, Chiba 260-8717, Japan. Fax: +81 43 265 4459 (T. Ozaki).

E-mail addresses: atakatori@chiba-cc.jp (A. Takatori), tozaki@chiba-cc.jp (T. Ozaki).

http://dx.doi.org/10.1016/j.bbrc.2014.09.065
0006-291X/